PFC/JA-84-36

INFLUENCE OF PROFILE SHAPE ON THE EXTRAORDINARY-MODE STABILITY PROPERTIES OF RELATIVISTIC NONNEUTRAL ELECTRON FLOW IN A PLANAR DIODE WITH APPLIED MAGNETIC FIELD

Ronald C. Davidson
Kang T. Tsang

October, 1984

INFLUENCE OF PROFILE SHAPE ON THE EXTRAORDINARY-MODE STABILITY PROPERTIES OF RELATIVISTIC NONNEUTRAL ELECTRON FLOW IN A PLANAR DIODE WITH APPLIED MAGNETIC FIELD

Ronald C. Davidson
Plasma Fusion Center
Massachusetts Institute of Technology, Cambridge, MA 02139

Kang T. Tsang
Science Applications Inc., Boulder, CO 80302

ABSTRACT

The cold-fluid extraordinary-mode eigenvalue equation is solved numerically to determine the influence of equilibrium profile shape on the detailed stability properties of relativistic nonneutral electron flow in a planar diode with cathode located at x=0 and anode at x=d. Stability properties are investigated for the class of equilibrium energy profiles $\gamma_b(x)$ specified by

$$\gamma_b(x) = \lambda\cosh\alpha_1 x + (1-\lambda)\frac{[1-\alpha_2^2(b^2-x^2)]^{1/2}}{[1-\alpha_2^2 b^2]^{1/2}}$$

over the interval $0\leq x\leq b$. Here, α_1 and α_2 are constants (with $\alpha_2^2 b^2<1$), x=b is the outer edge of the electron layer, and λ is a constant parameter in the range of $0\leq\lambda\leq 1$. The corresponding equilibrium profiles for $B_z(x)$, $n_b(x)$ and $E_x(x)$ are determined self-consistently from the steady-state ($\partial/\partial t=0$) cold-fluid-Maxwell equations. As the parameter λ is varied from unity to zero there is a large change in the equilibrium profile for $n_b(x)/\gamma_b(x)$, ranging from $n_b(x)/\gamma_b(x)$=const. over the interval $0\leq x<b$ when $\lambda=1$, to monotonic decreasing profiles for $n_b(x)/\gamma_b(x)$ when $\lambda<1$. The numerical analysis of the extraordinary-mode eigenvalue equation shows that the detailed stability properties are very sensitive to the shape of the equilibrium profiles. As λ is reduced from unity, and the profile for $n_b(x)/\gamma_b(x)$ becomes monotonic decreasing, it is found that the instability growth rate $\mathrm{Im}\omega$ is reduced. Moreover, the greater the monotonicity of $n_b(x)/\gamma_b(x)$ (i.e., the smaller the value of λ), the more the growth rate is reduced. Indeed, in some parameter regimes, the instability growth rate can be reduced to zero over the range of wavenumber k examined numerically.

I. INTRODUCTION AND SUMMARY

There is a growing literature[1-8] on theoretical studies of the equilibrium and stability properties of sheared, nonneutral electron flow in cylindrical and planar models of high-voltage diodes with application to the generation of intense charged particle beams for inertial confinement fusion.[9,10] These analyses[1-8] have represented major extensions of earlier work[11-18] to include the important influence of relativistic,[1-4] electromagnetic,[1-4] cylindrical,[5] nonlinear,[6] and kinetic[7,8] effects on equilibrium and stability properties at moderately high electron density. The majority[1-6] of these recent studies have been based on macroscopic cold-fluid models, largely for reasons of analytical and numerical convenience. In the present article, we make use of the extraordinary-mode eigenvalue equation derived in Ref. 1 to investigate the stability properties of relativistic, sheared, nonneutral electron flow in a high-voltage diode with applied magnetic field $B_0\hat{e}_z$ (Fig. 1). Particular emphasis is placed on determining the sensitivity of detailed stability properties to the shape of the equilibrium profiles for density $n_b(x)$, energy $\gamma_b(x)mc^2$, flow velocity $V_y(x) = -cE_x(x)/B_z(x)$, etc.

To briefly summarize, the equilibrium and stability analysis (Secs. II and III) is based on the cold-fluid-Maxwell equations for extraordinary-mode field perturbations (δE_x, δE_y, δB_z) in the planar diode configuration illustrated in Fig. 1. The cathode is located at $x = 0$, the anode is located at $x = d$, and the equilibrium density profile $n_b(x)$ extends from $x = 0$

(the cathode) to $x=b$ (the edge of the electron layer). Space-charge-limited flow with $E_x(x=0)=0$ is assumed, and the equilibrium magnetic field $B_z(x)$ in the vacuum region ($b<x\leq d$) is equal to the externally applied magnetic field $B_0=\text{const}$. All of the equilibrium quantities $n_b(x)$, $\gamma_b(x)$, $E_x(x)$, $B_z(x)$, and $V_y(x)$ $-cE_x(x)/B_z(x)$ of course are related self-consistently through the Maxwell equations (3) and (4) [see also Eqs. (1), (2) and (5) - (9)].[1-4]

In the numerical analysis (Sec. III) of the extraordinary-mode eigenvalue equation (12), it is assumed that the equilibrium profile for $\gamma_b(x)=[1-E_x^2(x)/B_z^2(x)]^{-1/2}$ is of the form [Eq. (16)]

$$\gamma_b(x)=\lambda\cosh\alpha_1 x+(1-\lambda)\frac{[1-\alpha_2^2(b^2-x^2)]^{1/2}}{[1-\alpha_2^2b^2]^{1/2}}$$

over the interval $0\leq x\leq b$. In Eq. (16), α_1 and α_2 are constants (with $\alpha_2^2b^2<1$), and λ is a constant parameter in the range $0\leq\lambda\leq 1$. Note from Eq. (16) that $\gamma_b(x)$ increases monotonically from $\gamma_b(0)=1$ at the cathode ($x=0$) to $\gamma_b(b)=\lambda\cosh\alpha_1 b+(1-\lambda)[1-\alpha_2^2b^2]^{-1/2}$ at the edge of the electron layer ($x=b$). The corresponding self-consistent profiles for $B_z(x)$, $n_b(x)$ and $E_x(x)$ are determined from Eqs. (7) - (9).

As the parameter λ is varied from zero to unity, there is a large change in the shape of the density profile $n_b(x)$ [Fig. 2]. For example, for $\lambda=1$, it is found that $n_b(x)/\gamma_b(x)=\text{const.}$ over the interval $0\leq x<b$ [Eq. (21)], corresponding to a density profile $n_b(x)$ that <u>increases</u> with increasing x. On the other hand,

for $\lambda<1$, it is found that $n_b(x)/\gamma_b(x)$ is monotonic decreasing over the interval $0\leq x<b$. Indeed, for $\lambda=0$, the equilibrium density profile satisfies $n_b(x)$=const. over the interval $0\leq x<b$ [Eq. (25)], corresponding to a density profile $n_b(x)$ that is <u>constant</u> out to the edge of the electron layer (x=b).

The analysis in Sec. III shows that detailed stability properties are very sensitive to the shape of the equilibrium profiles [Figs. 3-9]. To briefly summarize, for the cases studied in Sec. III, it is found that $\lambda=1$ corresponds to the strongest instability for fixed values of $\gamma_b(b)$, $b\omega_c/c$, $\hat{s}$ and $d\omega_c/c$. Here, $\omega_c \equiv eB_0/\gamma_b(b)mc$ is the relativistic cyclotron frequency, and $\hat{s} \equiv 4\pi\bar{n}_b e^2/\gamma_b(b)m\omega_c^2$ is a measure of the average density $\bar{n}_b = \int_0^b (dx/b)n_b(x)$. On the other hand, as λ is reduced from unity, and the profile for $n_b(x)/\gamma_b(x)$ becomes monotonic decreasing, it is found that the instability growth rate $\mathrm{Im}\omega$ is reduced. Indeed, in some parameter regimes, the instability growth rate can be reduced to zero over the range of wavenumber k examined numerically in Sec. III.

We conclude that detailed stability properties exhibit a very sensitive dependence on profile shape. Evidently, the greater the monotonicity of $n_b(x)/\gamma_b(x)$ (i.e., the smaller the value of λ), the more the growth rate is reduced. On the other hand, for fixed values of $\gamma_b(b)$, $d\omega_c/c$, and $\hat{s}b\omega_c/c=$ const., it is found that the real oscillation frequency $\mathrm{Re}\omega$ is relatively insensitive to profile shape. As in previous studies,[1-3] the growth rate $\mathrm{Im}\omega$ tends to decrease as the average electron density ($\hat{s}$) is reduced.

II. SUMMARY OF THEORETICAL MODEL

We consider relativistic electron flow in the planar diode configuration illustrated in Fig. 1. The cathode is located at $x = 0$ and the anode is located at $x = d$. The equilibrium and stability analysis is based on the macroscopic cold-fluid-Maxwell equations assuming negligibly small electron pressure.[1-4]

A. Equilibrium Properties

Denoting the steady-state $(\partial/\partial t = 0)$ electric and magnetic fields by $\underset{\sim}{E}_0(\underset{\sim}{x}) = E_x(x)\hat{\underset{\sim}{e}}_x$ and $\underset{\sim}{B}_0(\underset{\sim}{x}) = B_z(x)\hat{\underset{\sim}{e}}_z$, the equilibrium $\underset{\sim}{E}_0 \times \underset{\sim}{B}_0$ flow velocity is in the y-direction with

$$V_y(x) = -c\,\frac{E_x(x)}{B_z(x)}\,, \tag{1}$$

where c is the speed of light in vacuo. Moreover, in equilibrium, the relativistic mass factor $\gamma_b(x)$ of an electron fluid element can be expressed as

$$\gamma_b(x) = \left[1 - \frac{E_x^2(x)}{B_z^2(x)}\right]^{-1/2} \tag{2}$$

in the region where the equilibrium electron density $n_b(x)$ is non-zero. In the present analysis, it is assumed that the electron density $n_b(x)$ extends from $x = 0$ (the cathode) to $x = b$ (the outer edge of the electron layer). The region between $x = b$ and $x = d$ is a vacuum region, where $B_z(z) = B_0 = \text{const.}$ is the externally applied magnetic field. Of course, the equilibrium electric and magnetic fields, $E_x(x)$ and $B_z(x)$, must be determined self-consistently from Maxwell's equations,

$$\frac{\partial}{\partial x} E_x(x) = -4\pi e n_b(x), \tag{3}$$

and

$$\frac{\partial}{\partial x} B_z(x) = \frac{4\pi e}{c} n_b(x) V_y(x), \tag{4}$$

where $-e$ is the electron charge, and $V_y = -cE_x/B_z$. For present purposes, we assume space-charge-limited flow with $E_x(x=0)=0$, $\phi_0(x=0)=0$ and $\phi_0(x=d)=V_s$. Here, V_s is the voltage at the anode, $\phi_0(x)$ is the electrostatic potential, and $E_x(x)=-\partial\phi_0(x)/\partial x$. For space-charge-limited flow with $E_x(x=0)=0$, it is readily shown from Eq. (3) that

$$E_x(x) = -4\pi e \int_0^x dx' n_b(x'), \tag{5}$$

and that the anode voltage is $V_s = \phi_0(x=d) = 4\pi e \int_0^d dx'' \int_0^{x''} dx' n_b(x')$. Moreover, combining Eqs. (3) and (4) gives $B_z^2(x) - E_x^2(x) = \text{const.}$, or equivalently

$$\frac{B_z(x)}{\gamma_b(x)} = \text{const.} \tag{6}$$

in the region where $n_b(x)$ is non-zero.

One approach[1] in describing the equilibrium properties of the electron layer is to specify the functional form of the electron density $n_b(x)$, and then calculate the corresponding profiles for $E_x(x)$, $B_z(x)$, $V_y(x)$ and $\gamma_b(x)$ self-consistently from Eqs. (1) - (6). Another approach, which is the one used here (see also Sec. III), is to specify the functional form of $\gamma_b(x)$ over the interval $0 \le x \le b$ where the electron density is non-zero, and then make use of Eqs. (1) - (6) to calculate the

remaining profiles. Let us assume that $\gamma_b(x)$ is prescribed over the interval $0 \leq x \leq b$, with $\gamma_b(x)$ increasing from unity at $x = 0$ to $\gamma_b(b)$ at $x = b$. It is readily shown from the preceding analysis that the corresponding self-consistent profiles for $B_z(x)$, $n_b(x)$ and $E_x(x)$ are given by

$$B_z(x) = \begin{cases} \gamma_b(x) \dfrac{B_0}{\gamma_b(b)}, & 0 \leq x \leq b, \\ B_0, & b \leq x \leq d, \end{cases} \tag{7}$$

$$n_b(x) = \begin{cases} \left\{ \dfrac{\partial}{\partial x} \left[\gamma_b^2(x) - 1 \right]^{1/2} \right\} \dfrac{B_0}{4\pi e \gamma_b(b)}, & 0 \leq x < b, \\ 0, & b < x \leq d, \end{cases} \tag{8}$$

and

$$E_x(x) = \begin{cases} -\left[\gamma_b^2(x) - 1 \right]^{1/2} \dfrac{B_0}{\gamma_b(b)}, & 0 \leq x \leq b, \\ E_x(b), & b \leq x \leq d. \end{cases} \tag{9}$$

Here $E_x(b) = -[\gamma_b^2(b) - 1]^{1/2} B_0/\gamma_b(b)$ and $B_z(b) = B_0$ are the fields in the vacuum region $b \leq x \leq d$. Moreover, $\gamma_b(b) = [1 - E_x^2(b)/B_0^2]^{-1/2}$ is the relativistic mass factor at the edge $(x = b)$ of the electron layer.

In the numerical analysis in Sec. III, we investigate extraordinary-mode stability properties for different choices of energy profile $\gamma_b(x)$. In this regard, it is important to note from Eq. (8) that the average electron density $\bar{n}_b = \int_0^b (dx/b) n_b(x)$ can be expressed as

$$\bar{n}_b = \left[\gamma_b^2(b) - 1\right]^{1/2} \frac{B_0}{4\pi e b \gamma_b(b)} ,$$

$$= - \frac{E_x(b)}{4\pi e b} . \tag{10}$$

Therefore, although the detailed shape of the density profile changes as the functional form of $\gamma_b(x)$ is varied, it is clear from Eq. (10) that the $\bar{n}_b$ can be maintained constant provided the value of $\gamma_b(b)$ is held fixed (assuming fixed values of B_0 and b).

B. Extraordinary-Mode Eigenvalue Equation

In the numerical analysis of stability properties in Sec. III, we make use of the eigenvalue equation derived in Ref. 1 for extraordinary-mode perturbations about general equilibrium density profile $n_b(x)$. To briefly summarize, we assume electromagnetic perturbations with perturbed field components $\delta\underset{\sim}{E}(\underset{\sim}{x},t) = \delta E_x(x,y,t)\hat{\underset{\sim}{e}}_x + \delta E_y(x,y,t)\hat{\underset{\sim}{e}}_y$ and $\delta\underset{\sim}{B}(\underset{\sim}{x},t) = \delta B_z(x,y,t)\hat{\underset{\sim}{e}}_z$. Here, $\partial/\partial z = 0$ is assumed, and perturbed quantities are expressed as $\delta\psi(x,y,t) = \delta\hat{\psi}(x)\ \exp(iky-i\omega t)$, where ω is the complex oscillation frequency, $k = 2\pi n/L$ is the wavenumber, and L is the periodicity length in the y-direction. It is convenient to introduce the effective potential $\Phi(x)$ defined by

$$\Phi(x) = \frac{i}{k}\ \delta\hat{E}_y(x) . \tag{11}$$

Then, making use of the linearized cold-fluid-Maxwell equations, it is found[1] that the eigenvalue equation for $\Phi(x)$ can be expressed as

$$\frac{\partial}{\partial x}\left\{\left[1+\chi_{\perp}(x,k,\omega)\right]\frac{\partial}{\partial x}\Phi\right\} - k^2\left[1+\chi_{\parallel}(x,k,\omega)\right]\Phi$$

$$= \frac{k\Phi}{[\omega - kV_y(x)]}\left[1-\frac{V_y(x)}{c}\frac{\omega}{ck}\right]\frac{\partial}{\partial x}\left[\frac{\omega_{pb}^2(x)\omega_c}{\nu_b^2(x,k,\omega)}\right] , \tag{12}$$

where $\omega_c = eB_z(x)/\gamma_b(x)mc = eB_0/\gamma_b(b)mc = \text{const.}$ is the relativistic cyclotron frequency, and $\omega_{pb}^2(x) = 4\pi n_b(x)e^2/\gamma_b(x)m$ is the relativistic plasma frequency-squared. Moreover, the effective susceptibilities are defined by[1]

$$\chi_{\perp}(x,k,\omega) = -\left[1-\frac{V_y(x)}{c}\frac{\omega}{ck}\right]^2 \frac{\omega_{pb}^2(x)\gamma_b^2(x)}{(1-\omega^2/c^2k^2)\nu_b^2(x,k,\omega)}, \tag{13}$$

$$\chi_{\parallel}(x,k,\omega) = -\frac{\omega^2}{c^2k^2} - \frac{\omega_{pb}^2(x)}{\nu_b^2(x,k,\omega)}\left[1-\frac{\omega^2}{c^2k^2}+\frac{\omega_{pb}^2(x)}{c^2k^2}\right] , \tag{14}$$

where

$$\nu_b^2(x,k,\omega) = \gamma_b^2(x)[\omega - kV_y(x)]^2\left[1+\frac{\omega_{pb}^2(x)/c^2k^2}{1-\omega^2/c^2k^2}\right] - [\omega_c^2 - \omega_{pb}^2(x)] . \tag{15}$$

The eigenvalue equation (12) can be used to investigate extraordinary-mode stability properties for a wide range of self-consistent equilibrium profiles $n_b(x)$, $\gamma_b(x)$, $V_y(x) = -cE_x(x)/B_z(x)$, and $B_z(x)$. Previous stability analyses have been restricted to the special class of equilibrium profiles where $n_b(x)/\gamma_b(x)$ = const. over the interval $0 \le x < b$. In Sec. III, we make use of Eq. (12) to determine stability properties for profiles ranging from $n_b(x)/\gamma_b(x) = \text{const.}$ to $n_b(x) = \text{const.}$ over the interval $0 \le x < b$.

III. STABILITY ANALYSIS

In this section, we make use of the eigenvalue equation (12) to investigate extraordinary-mode stability properties for a range of equilibrium profiles in order to determine the sensitivity of stability behavior to profile shape.

A. Model Equilibrium Profiles

In the present analysis, we choose $\gamma_b(x)$ to have the functional form

$$\gamma_b(x) = \lambda \cosh\alpha_1 x + (1-\lambda)\,\frac{[1-\alpha_2^2(b^2-x^2)]^{1/2}}{(1-\alpha_2^2 b^2)^{1/2}} \tag{16}$$

over the interval $0 \le x \le b$. In Eq. (16), α_1 and α_2 are constants (with $\alpha_2^2 b^2 < 1$), and λ is a constant parameter in the range $0 \le \lambda \le 1$. We note from Eq. (16) that $\gamma_b(x=0) = 1$, as required, and that $\gamma_b(x)$ increases monotonically as x is increased from $x=0$ to $x=b$. Moreover, it is evident that λ and $\gamma_b(b)$ are related by

$$\gamma_b(b) = \lambda \cosh\alpha_1 b + (1-\lambda)/(1-\alpha_2^2 b^2)^{1/2}. \tag{17}$$

The corresponding profiles for $B_z(x)$, $n_b(x)$ and $E_x(x)$, consistent with Eq. (16), are readily obtained by substituting Eq. (16) into Eqs. (7)-(9). To illustrate the range of profile shapes modelled by Eq. (16), it is instructive to consider two limiting cases: (a) $\lambda = 1$, and (b) $\lambda = 0$.

(a) $\lambda = 1$: Rectangular Profile for $n_b(x)/\gamma_b(x)$: For $\lambda = 1$, it follows from Eqs. (16) and (17) that[1-4]

$$\gamma_b(x) = \cosh\alpha_1 x \tag{18}$$

over the interval $0 \leq x \leq b$, and that $\gamma_b(b) = \cosh\alpha_1 b$. Moreover, Eqs. (7) and (9) give for the equilibrium fields,[1-4]

$$B_z(x) = \begin{cases} \dfrac{\cosh\alpha_1 x}{\cosh\alpha_1 b} B_0, & 0 \leq x \leq b, \\ B_0, & b \leq x \leq d, \end{cases} \tag{19}$$

and

$$E_x(x) = \begin{cases} -\dfrac{\sinh\alpha_1 x}{\cosh\alpha_1 b} B_0, & 0 \leq x \leq b, \\ -\dfrac{\sinh\alpha_1 b}{\cosh\alpha_1 b} B_0, & b \leq x \leq d. \end{cases} \tag{20}$$

Similarly, substituting Eq. (18) into Eq. (8), we find the rectangular profile

$$\frac{n_b(x)}{\gamma_b(x)} = \begin{cases} \dfrac{\alpha_1 B_0}{4\pi e \gamma_b(b)} = \text{const.}, & 0 \leq x < b, \\ 0, & b < x \leq d \end{cases} \tag{21}$$

for $n_b(x)/\gamma_b(x)$. As indicated earlier, extraordinary-mode stability properties have been investigated in the literature[1-4] for the special class of profiles in Eqs. (18)-(21), which corresponds to $\lambda = 1$ and $\omega_{pb}^2(x) = \text{const.}$ over the interval $0 \leq x < b$.

(b) <u>$\lambda = 0$: Rectangular Profile for $n_b(x)$:</u> For $\lambda = 0$, Eq. (16) reduces to (for $0 \leq x \leq b$)

$$\gamma_b(x) = \frac{[1 - \alpha_2^2(b^2 - x^2)]^{1/2}}{(1 - \alpha_2^2 b^2)^{1/2}}, \tag{22}$$

where $\gamma_b(b) = 1/(1-\alpha_2^2 b^2)^{1/2}$. From Eqs. (7) and (9), the equilibrium field profiles corresponding to Eq. (22) are given by

$$B_z(x) = \begin{cases} [1-\alpha_2^2(b^2-x^2)]^{1/2}B_0, & 0\leq x\leq b, \\ B_0, & b\leq x\leq d, \end{cases} \tag{23}$$

and

$$E_x(x) = \begin{cases} -\alpha_2 x B_0, & 0\leq x\leq b, \\ -\alpha_2 b B_0, & b\leq x\leq d. \end{cases} \tag{24}$$

Moreover, from Eqs. (8) and (22), the equilibrium density $n_b(x)$ is given by

$$n_b(x) = \begin{cases} \dfrac{\alpha_2 B_0}{4\pi e} = \text{const.}, & 0\leq x<b, \\ 0, & b<x\leq d, \end{cases} \tag{25}$$

which corresponds to a rectangular profile for $n_b(x)$ when $\lambda = 0$. This should be contrasted with the $\lambda = 1$ case, where $n_b(x)/\gamma_b(x)$ has a rectangular profile [Eq. (21)] and therefore $n_b(x)$ <u>increases</u> over the interval $0\leq x<b$.

Making use of Eqs. (7)-(9) and (16), shown in Fig. 2 are illustrative plots of $\gamma_b(x)$, $n_b(x)$, $n_b(x)/\gamma_b(x)$, $B_z(x)$, $E_x(x)$ and $V_y(x) = -cE_x(x)/B_z(x)$. The equilibrium profiles are plotted versus x/b for the choice of parameters: $\gamma_b(b) = 2$, $\alpha_1 b = 1.317$ [corresponding to $\cosh(\alpha_1 b) = 2$], $\alpha_2 b = 0.866$ [corresponding to $(1-\alpha_2^2 b^2)^{-1/2} = 2$], and values of λ, including $\lambda = 0$, $\lambda = 0.5$ and

$\lambda = 1$. Although the changes in $\gamma_b(x)$, $B_z(x)$, $E_x(x)$ and $V_y(x) = -cE_x(x)/B_z(x)$ are relatively small [Figs. 2(a)-2(c)] as λ is varied from $\lambda = 1$ to $\lambda = 0$, it is clear from Figs. 2(d) and 2(e) that there are large variations in $n_b(x)$ and $n_b(x)/\gamma_b(x)$ as λ is changed. For example, from Fig. 2(e), $n_b(x)/\gamma_b(x) = \text{const.}$ over the interval $0 \leq x < b$ when $\lambda = 1$. On the other hand, when $\lambda = 0$, $n_b(x)/\gamma_b(x)$ decreases monotonically by a factor of two from the cathode $(x = 0)$ to the outer edge of the electron layer $(x = b)$.

B. Numerical Results and Discussion

In this section, the extraordinary-mode eigenvalue equation (12) is solved numerically to determine the influence of equilibrium profile shape on detailed stability properties. The equilibrium profile for $\gamma_b(x)$ is specified by Eq. (16), and the corresponding profiles for $E_x(x)$, $n_b(x)$, $B_z(x)$ and $V_y(x) = -cE_x(x)/B_z(x)$ are calculated self-consistently from Eqs. (7) - (9). In the present analysis, $\alpha_1 b$ and $\alpha_2 b$ are specified in terms of $\gamma_b(b)$ by

$$\cosh\alpha_1 b = \gamma_b(b),$$
$$(1 - \alpha_2^2 b^2)^{-1/2} = \gamma_b(b). \tag{26}$$

From Eq. (26), note that Eq. (17) is automatically satisfied for λ in the range $0 \leq \lambda \leq 1$. The eigenvalue equation (12) is solved numerically for the complex eigenfunction $\Phi(x) = (i/k)\delta\hat{E}_y(x)$ and eigenfrequency ω subject to the boundary conditions

$$\Phi(x=0) = 0 = \Phi(x=d). \tag{27}$$

In the numerical analysis of Eq. (12), λ is varied from zero to unity, corresponding to a large change in the equilibrium profiles for $n_b(x)$ and $n_b(x)/\gamma_b(x)$ [see Figs. 2(d) and 2(e)]. Moreover, we introduce the dimensionless quantity $s(x)$ defined by

$$s(x) = \frac{\omega_{pb}^2(x)}{\omega_c^2} = \hat{s}\left[\frac{n_b(x)}{\gamma_b(x)} \cdot \frac{\gamma_b(b)}{\bar{n}_b}\right], \tag{28}$$

where $\hat{s}$ is defined by

$$\hat{s} \equiv \frac{4\pi\bar{n}_b e^2}{\gamma_b(b)m\omega_c^2}. \tag{29}$$

Here, $\omega_c = eB_0/\gamma_b(b)mc$ is the relativistic cyclotron frequency, and $\bar{n}_b = \int_0^b (dx/b)n_b^0(x)$ is the average electron density [Eq. (10)]. In comparing stability properties for different profile shapes (i.e., different values of λ), we will specify values for $\gamma_b(b)$ and $b\omega_c/c$, which corresponds to fixing the value of $\hat{s}$. The shape function

$$f(x) \equiv \frac{n_b(x)}{\gamma_b(x)} \quad \frac{\gamma_b(b)}{\bar{n}_b} \tag{30}$$

occurring in Eq. (29), however, varies substantially as the parameter λ is changed. For example, for the parameters in Fig. 2(e), it follows for $\lambda = 1$ that $f(x) = \text{const.} = 1.52$ over the interval $0 \leq x \leq b$. On the other hand, for $\lambda = 0$, $f(x)$

decreases monotonically from $f(0) = 2$ at the cathode $(x = 0)$ to $f(b) = 1$ at the outer edge of the electron layer $(x = b)$. As a final point, before discussing the numerical results, the relation between $\gamma_b(b)$, $\hat{s}$ and $b\omega_c/c$ is readily derived. Making use of $\gamma_b(b) = [1 - E_x^2(b)/B_0^2]^{-1/2}$ and $E_x(b) = -4\pi e\bar{n}_b b$, we find

$$\hat{s}^2 \frac{b^2\omega_c^2}{c^2} = 1 - \frac{1}{\gamma_b^2(b)} , \tag{31}$$

where $\hat{s}$ is defined in Eq. (29). Therefore, upon specifying values for $b\omega_c/c$ and $\gamma_b(b)$, we obtain the corresponding self-consistent value of $\hat{s}$ from Eq. (31).

Typical numerical results obtained from the eigenvalue equation (12) are shown in Figs. 3 - 7 for the choice of parameters

$$\begin{aligned} \gamma_b(b) &= 4, \; d\omega_c/c = 3, \\ \alpha_1 b &= 2.0635, \; \alpha_2 b = 0.9682. \end{aligned} \tag{32}$$

Here, $\gamma_b(x)$ is specified by Eq. (16), and the corresponding equilibrium profiles for $B_z(x)$, $n_b(x)$ and $E_x(x)$ are calculated self-consistently from Eqs. (7) - (9). In Figs. 3 - 5, the normalized growth rate $\mathrm{Im}\omega/\omega_c$ is plotted versus kc/ω_c for $(b\omega_c/c, \hat{s}) = (0.5, 1.936)$ [Fig. 3], $(b\omega_c/c, \hat{s}) = (1, 0.968)$ [Fig. 4], $(b\omega_c/c, \hat{s}) = (2, 0.484)$ [Fig. 5], and several values of the profile shape parameter λ. For $\gamma_b(b) = 4$ and fixed value of applied magnetic field B_0, we note that the different cases studied in Figs. 3 - 5 correspond to $\hat{s}b\omega_c/c = 0.968 = \text{const.}$ and therefore $\bar{n}_b b = \text{const.}$ That is, as the layer thickness is

increased from Fig. 3 through Fig. 5, the average electron density $\bar{n}_b$ is decreased so that $\bar{n}_b b$ remains constant. It is evident from Fig. 3, which correponds to $(b\omega_c/c, \hat{s}) = (0.5, 1.936)$, that the growth rate decreases by more than a factor of two as λ is decreased from $\lambda=1$ to $\lambda=0$. That is, as the profile for $n_b(x)/\gamma_b(x)$ is varied from a rectangular profile ($\lambda=1$) to a monotonic decreasing profile ($\lambda=0.5$ and $\lambda=0$), there is a concommitant decrease in instability growth rate.

The effect is even more dramatic in Figs. 4 and 5. In Fig. 4, which corresponds to $(b\omega_c/c, \hat{s}) = (1, 0.968)$, we first note that the growth rates are reduced relative to Fig. 3 because of the lower electron density (smaller $\hat{s}$). Moreover, the growth rate in Fig. 4 also decreases as the profile for $n_b(x)/\gamma_b(x)$ becomes more monotonic (i.e., as λ is decreased). The most striking feature of the stability results in Fig. 4 is that the system stabilizes for λ below some critical value. In particular, for the choice of parameters in Fig. 4, instability ceases for $\lambda \lesssim 0.12$ over the entire range of kc/ω_c investigated numerically ($kc/\omega_c \leq 5$). The results are qualitatively similar for the case shown in Fig. 5, which corresponds to $(b\omega_c/c, \hat{s}) = (2, 0.484)$. As in Figs. 3 and 4, the instability growth rate in Fig. 5 decreases as the profiles for $n_b(x)/\gamma_b(x)$ become more monotonic (i.e., as λ is decreased). Moreover, for the choice of parameters in Fig. 5, instability ceases for $\lambda \lesssim 0.38$ over the entire range of kc/ω_c investigated numerically ($kc/\omega_c \leq 5$).

We conclude from Figs. 3 - 5 that detailed stability properties exhibit a very sensitive dependence on profile shape. Evidently, the greater the monotonicity of $n_b(x)/\gamma_b(x)$ (i.e., the

smaller the value of λ), the more the growth rate is reduced. Indeed, in some parameter regimes, the instability growth rate can be reduced to zero, even at moderate electron density (see Figs. 4 and 5). It is also evident from Figs. 3 - 5 that the growth rate $\mathrm{Im}\omega$ tends to achieve a maximum value at increasingly large values of k as the parameter λ is reduced. For example, it is found numerically that the $\lambda = 0.25$ growth curve in Fig. 4 achieves a maximum value of $\mathrm{Im}\omega \simeq 0.018\omega_c$ for $kc/\omega_c \approx 30$.

Shown in Fig. 6 is a plot of normalized real frequency $\mathrm{Re}\omega/\omega_c$ versus ck/ω_c for the choice of parameters in Eq. (32) and $(b\omega_c/c, \hat{s}, \lambda) = (1, 0.968, 1)$. Note that $\mathrm{Re}\omega$ increases approximately linearly with k with $(\mathrm{Re}\omega)/k \simeq 0.89\ V_y(b) \simeq 0.86\ c$ over the range of unstable k-values. The parameters chosen in Fig. 6 correspond to the most unstable case (λ=1) analyzed in Fig. 4. Moreover, for $\gamma_b(b) = 4$ and $d\omega_c/c = 3$ [Eq. (32)], it is found that the plots of $\mathrm{Re}\omega/\omega_c$ versus ck/ω_c are virtually identical to Fig. 6 for all other values of $(b\omega_c/c, \hat{s}, \lambda)$ analyzed in Figs. 3 - 5. Therefore, although the growth rate $\mathrm{Im}\omega$ is very sensitive to the profile shape (λ) and the value of $\hat{s}$, we conclude that the real frequency $\mathrm{Re}\omega$ is relatively insensitive to profile shape and $\hat{s}$, at least for $\hat{s}b\omega_c/c = \mathrm{const}$.

Shown in Fig. 7 are plots of $\mathrm{Re}\Phi$ and $\mathrm{Im}\Phi$ versus $x\omega_c/c$ obtained from Eq. (12) for $\gamma_b(b) = 4$, $b\omega_c/c = 1$, $d\omega_c/c = 3$, $\hat{s} = 0.968$, $kc/\omega_c = 3$, and several values of the profile shape parameter λ. The corresponding plots of $\mathrm{Im}\omega/\omega_c$ and $\mathrm{Re}\omega/\omega_c$ versus kc/ω_c are given in Figs. 4 and 6. Note from Figs. 7(a) - 7(c) that the outer extremum of $\mathrm{Re}\Phi(x)$ occurs near the boundary of

the plasma $(x=b)$ where $\partial\omega_{pb}^2(x)/\partial x$ is large, corresponding to a large surface perturbation on the right-hand side of the eigenvalue equation (12). The strong peaking of $\mathrm{Re}\Phi(x)$ at $x=b$ is expected[1] since it is this large variation in $\omega_{pb}^2(x)$ at the plasma boundary which supports the slow surface wave that is driven unstable by equilibrium velocity shear. Close examination of the numerical results and the eigenvalue equation (12) shows that the inner extrema of $\mathrm{Re}\Phi(x)$ and $\mathrm{Im}\Phi(x)$ occur near the innermost point $(x=x_i)$ where $1+\mathrm{Re}\chi_\perp(x_i,k,\omega)=0$. After some straightforward algebra that makes use of Eqs. (13) and (15), it can be shown that

$$1 + \chi_\perp(x,k,\omega) = \frac{\gamma_b^2(x)\,[\omega - kV_y(x)]^2 - \omega_c^2}{\nu_b^2(x,k,\omega)} . \tag{33}$$

For small growth rate with $|\mathrm{Im}\omega| << |\mathrm{Re}\omega|$, the solution (x_i) to $1+\mathrm{Re}\chi_\perp(x_i,k,\omega)=0$ is determined approximately from the cyclotron resonance condition[1]

$$[\omega - kV_y(x_i)]^2 = \omega_c^2/\gamma_b^2(x_i) .$$

We note from Figs. 7(a) - 7(c) that there is a tendancy for x_i to move inward (toward the cathode) as λ is decreased. This is a result of the changes in the profiles for $V_y(x)$ and $\gamma_b(x)$ as the parameter λ is varied.

Finally, in Figs. 8 and 9 we illustrate typical stability results obtained from Eq. (12) for the choice of parameters

$$\begin{aligned} \gamma_b(b) &= 2, \ d\omega_c/c = 3 \\ \alpha_1 b &= 1.319, \ \alpha_2 b = 0.866. \end{aligned} \tag{35}$$

In particular, the normalized growth rate $\mathrm{Im}\omega/\omega_c$ [Fig. 8] and real frequency $\mathrm{Re}\omega/\omega_c$ [Fig. 9] are plotted versus ck/ω_c for $b\omega_c/c = 1$ and $\hat{s} = 0.866$. Comparing Fig. 4 [$\gamma_b(b) = 4$ and $b\omega_c/c = 1$] with Fig. 8 [$\gamma_b(b) = 2$ and $b\omega_c/c = 1$], it is evident that the growth rate $\mathrm{Im}\omega$ still exhibits a very sensitive dependence on profile shape (λ) as the relativistic mass factor $\gamma_b(b)$ is reduced from $\gamma_b(b) = 4$ to $\gamma_b(b) = 2$. That is, as the profile for $n_b(x)/\gamma_b(x)$ is varied from a rectangular profile ($\lambda = 1$) to a monotonic decreasing profile ($\lambda = 0.5$, 0.25 and 0.1), there is a significant reduction in the growth rate. Moreover, the real frequency $\mathrm{Re}\omega$ increases approximately linearly with k [Fig. 9], and is relatively insensitive to the value of λ. For the parameters in Figs. 8 and 9, it is found that instability ceases for $\lambda \lesssim 0.06$ over the range of kc/ω_c investigated numerically ($kc/\omega_c \leq 5$).

IV. CONCLUSIONS

In this paper, we have made use of the extraordinary-mode eigenvalue equation derived in Ref. 1 to determine the influence of equilibrium profile shape on the detailed stability properties of relativistic, nonneutral electron flow in a planar diode. The stability analysis is fully electromagnetic, and the relativistic cold-fluid model for the electrons includes the effects of equilibrium self fields in a self-consistent manner. Following a summary of the theoretical model (Sec. II), we investigated numerically the stability properties for a wide range of equilibrium profile shapes (Sec. III). To briefly summarize, the extraordinary-mode eigenvalue equation (12) was solved numerically for the class of equilibrium energy profiles $\gamma_b(x)$ specified by Eq. (16). The corresponding self-consistent profiles for $B_z(x)$, $n_b(x)$ and $E_x(x)$ were determined from Eqs. (7) - (9). As the profile shape parameter λ in Eq. (16) is varied from zero to unity, there is a large change in the equilibrium profile for $n_b(x)$ and in the equilibrium profile for $n_b(x)/\gamma_b(x)$ [Fig. 2]. For the cases studied in Sec. III, it is evident from Figs. 3 - 5 and 8, that $\lambda = 1$ corresponds to the strongest instability for fixed values of $\gamma_b(b)$, $b\omega_c/c$, $\hat{s}$ and $d\omega_c/c$. On the other hand, as λ is reduced from unity, and the profile for $n_b(x)/\gamma_b(x)$ become monotonic decreasing, the instability growth rate is reduced. Indeed, in some parameter regimes, the instability growth rate can be reduced to zero over the range of k examined numerically. [See Figs. 4 and 5 and the related discussion in Sec. III.]

We conclude that detailed stability properties exhibit a very sensitive dependence on the equilibrium profile shape. Evidently, the greater the monotonicity of $n_b(x)/\gamma_b(x)$ (i.e., the smaller the value of λ), the more the growth rate $\mathrm{Im}\omega$ is reduced. On the other hand, for fixed values of $\gamma_b(b)$, $d\omega_c/c$, and $\hat{s}b\omega_c/c = \text{const.}$, it is found that the real oscillation frequency $\mathrm{Re}\omega$ is relatively insensitive to profile shape (λ). As in previous studies,[1-3] the growth rate $\mathrm{Im}\omega$ tends to decrease as the average electron density ($\hat{s}$) is reduced. [Compare the stability behavior in Figs. 3 - 5.]

ACKNOWLEDGMENTS

This research was supported by Sandia National Laboratories and in part by the Office of Naval Research.

REFERENCES

1. R.C. Davidson, K.T. Tsang and J.A. Swegle, Phys. Fluids 27, 2332 (1984).

2. J. Swegle, Phys. Fluids 26, 1670 (1983).

3. J. Swegle and E. Ott, Phys. Fluids 24, 1821 (1981).

4. J. Swegle and E. Ott, Phys. Rev. Lett. 46, 929 (1981).

5. R.C. Davidson and K.T. Tsang, Phys. Rev. A29, 488 (1984).

6. R.C. Davidson, "Quasilinear Theory of Diocotron Instability for Nonrelativistic Nonneutral Electron Flow in Planar Diode with Applied Magnetic Field," submitted for publication (1984).

7. R.C. Davidson, Phys. Fluids 27, in press (1984).

8. H.S. Uhm and R.C. Davidson, "Kinetic Equilibrium Properties of Relativistic Nonneutral Electron Flow in a Cylindrical Diode with Applied Magnetic Field," submitted for publication (1984).

9. J.P. VanDevender, J.P. Quintenz, R.J. Leeper, D.J. Johnson and J.T. Crow, J. Appl. Phys. 52, 4 (1981).

10. R.B. Miller, Intense Charged Particle Beams (Plenum, New York, 1982).

11. O. Buneman, Proc. Cambridge Phil. Soc. 50, 77 (1954).

12. R.H. Levy, Phys. Fluids 8, 1288 (1965).

13. O. Buneman, R.H. Levy and L.M. Linson, J. Appl. Phys. 37, 3203 (1966).

14. R.J. Briggs, J.D. Daugherty and R.H. Levy, Phys. Fluids 13, 421 (1970).

15. C.A. Kapetanakos, D.A. Hammer, C.D. Striffler and R.C. Davidson, Phys. Rev. Lett. 30, 1303 (1973).

16. R.C. Davidson, Theory of Nonneutral Plasmas (Benjamin, Reading, Mass., 1974) pp. 17-89.

17. V.S. Voronen and A.N. Lebedev, Zh. Tekh. Fiz. 43, 2591 (1973) [Sov. Phys.-Tech. Phys. 18, 1627 (1974).

18. E. Ott and R.V. Lovelace, Appl. Phys. Lett. 27, 378 (1975).

FIGURE CAPTIONS

Fig. 1. Planar diode configuration and coordinate system.

Fig. 2. Illustrative equilibrium profiles based on Eqs. (1)-(9) with $\gamma_b(x)$ specified by Eq. (16). The parameters chosen are: $\gamma_b(b) = 2$; $\alpha_1 b = 1.317$ corresponding to $\cosh\alpha_1 b = 2$; $\alpha_2 b = 0.866$ corresponding to $(1 - \alpha_2^2 b^2)^{-1/2} = 2$; and $\lambda = 0$, 0.5 and 1. Plotted versus x/b are: (a) $\gamma_b(x)/\gamma_b(b)$ and $B_z(x)/B_0$ [Eqs. (16) and (7)], (b) $-E_x(x)/B_0$ [Eq. (9)], (c) $V_y(x)/c = -E_x(x)/B_z(x)$ [Eqs. (7) and (9)], (d) $n_b(x)/\bar{n}_b$ [Eqs. (8) and (10)], and (e) $[n_b(x)/\gamma_b(x)]\cdot[\gamma_b(b)/\bar{n}_b]$ [Eqs. (8) and (16)].

Fig. 3. Plots of $\mathrm{Im}\omega/\omega_c$ versus kc/ω_c obtained from Eq. (12) for $b\omega_c/c = 0.5$, $\gamma_b(b) = 4$, $d\omega_c/c = 3$, $\hat{s} = 1.936$, and (a) $\lambda = 1$, (b) $\lambda = 0.5$, and (c) $\lambda = 0$.

Fig. 4. Plots of $\mathrm{Im}\omega/\omega_c$ versus kc/ω_c obtained from Eq. (12) for $b\omega_c/c = 1$, $\gamma_b(b) = 4$, $d\omega_c/c = 3$, $\hat{s} = 0.968$, and (a) $\lambda = 1$, (b) $\lambda = 0.5$, and (c) $\lambda = 0.25$.

Fig. 5. Plots of $\mathrm{Im}\omega/\omega_c$ versus kc/ω_c obtained from Eq. (12) for $b\omega_c/c = 2$, $\gamma_b(b) = 4$, $d\omega_c/c = 3$, $\hat{s} = 0.484$, and (a) $\lambda = 1$, (b) $\lambda = 0.75$, and (c) $\lambda = 0.5$.

Fig. 6. Plot of $\mathrm{Re}\omega/\omega_c$ versus kc/ω_c obtained from Eq. (12) for $b\omega_c/c = 1$, $\gamma_b(b) = 4$, $d\omega_c/c = 3$, $\hat{s} = 0.968$, and $\lambda = 1$. (See also plot of $\mathrm{Im}\omega/\omega_c$ versus kc/ω_c for $\lambda = 1$ in Fig. 4.)

Fig. 7. Plots of $\mathrm{Re}\Phi$ and $\mathrm{Im}\Phi$ versus $x\omega_c/c$ obtained from Eq. (12) for $b\omega_c/c = 1$, $\gamma_b(b) = 4$, $d\omega_c/c = 3$, $\hat{s} = 0.968$, $kc/\omega_c = 3$, and (a) $\lambda = 1$ ($\mathrm{Re}\omega/\omega_c = 2.743$ and $\mathrm{Im}\omega/\omega_c = 0.03781$), (b) $\lambda = 0.5$, ($\mathrm{Re}\omega/\omega_c = 2.757$ and $\mathrm{Im}\omega/\omega_c = 0.0183$), and (c) $\lambda = 0.25$ ($\mathrm{Re}\omega/\omega_c = 2.761$ and $\mathrm{Im}\omega/\omega_c = 0.002431$).

Fig. 8 Plots of $\mathrm{Im}\omega/\omega_c$ versus kc/ω_c obtained from Eq. (12) for $b\omega_c/c = 1$, $\gamma_b(b) = 2$, $d\omega_c/c = 3$, $\hat{s} = 0.866$, and (a) $\lambda = 1$, (b) $\lambda = 0.5$, (c) $\lambda = 0.25$, and (d) $\lambda = 0.1$.

Fig. 9 Plot of $\mathrm{Re}\omega/\omega_c$ versus kc/ω_c obtained from Eq. (12) for $b\omega_c/c = 1$, $\gamma_b(b) = 2$, $d\omega_c/c = 3$, $\hat{s} = 0.866$ and $\lambda = 1$. (See also plot of $\mathrm{Im}\omega/\omega_c$ versus kc/ω_c for $\lambda = 1$ in Fig. 8.)

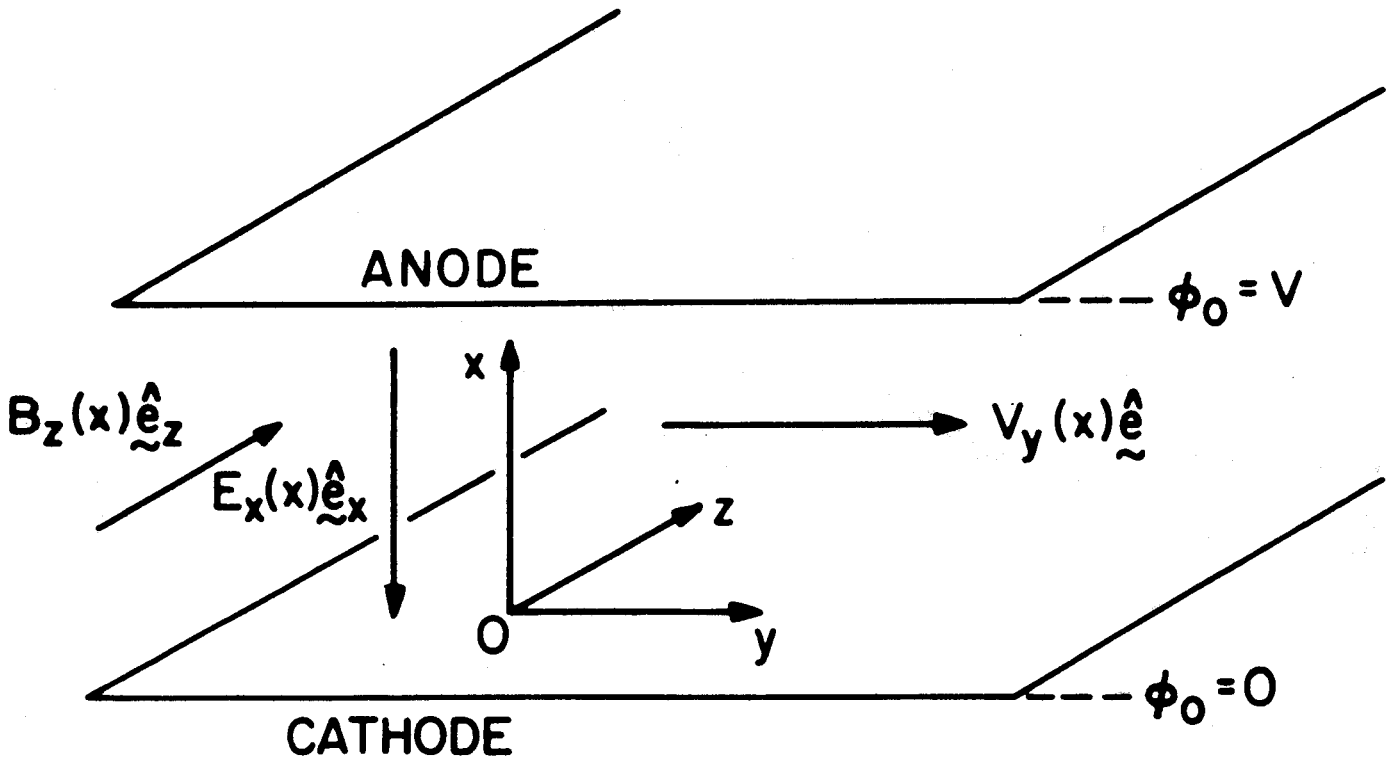
ANODE
$\phi_0 = V$
$B_z(x)\hat{\underset{\sim}{e}}_z$
$E_x(x)\hat{\underset{\sim}{e}}_x$
x
z
O
y
$V_y(x)\hat{\underset{\sim}{e}}$
$\phi_0 = 0$
CATHODE

Fig. 1

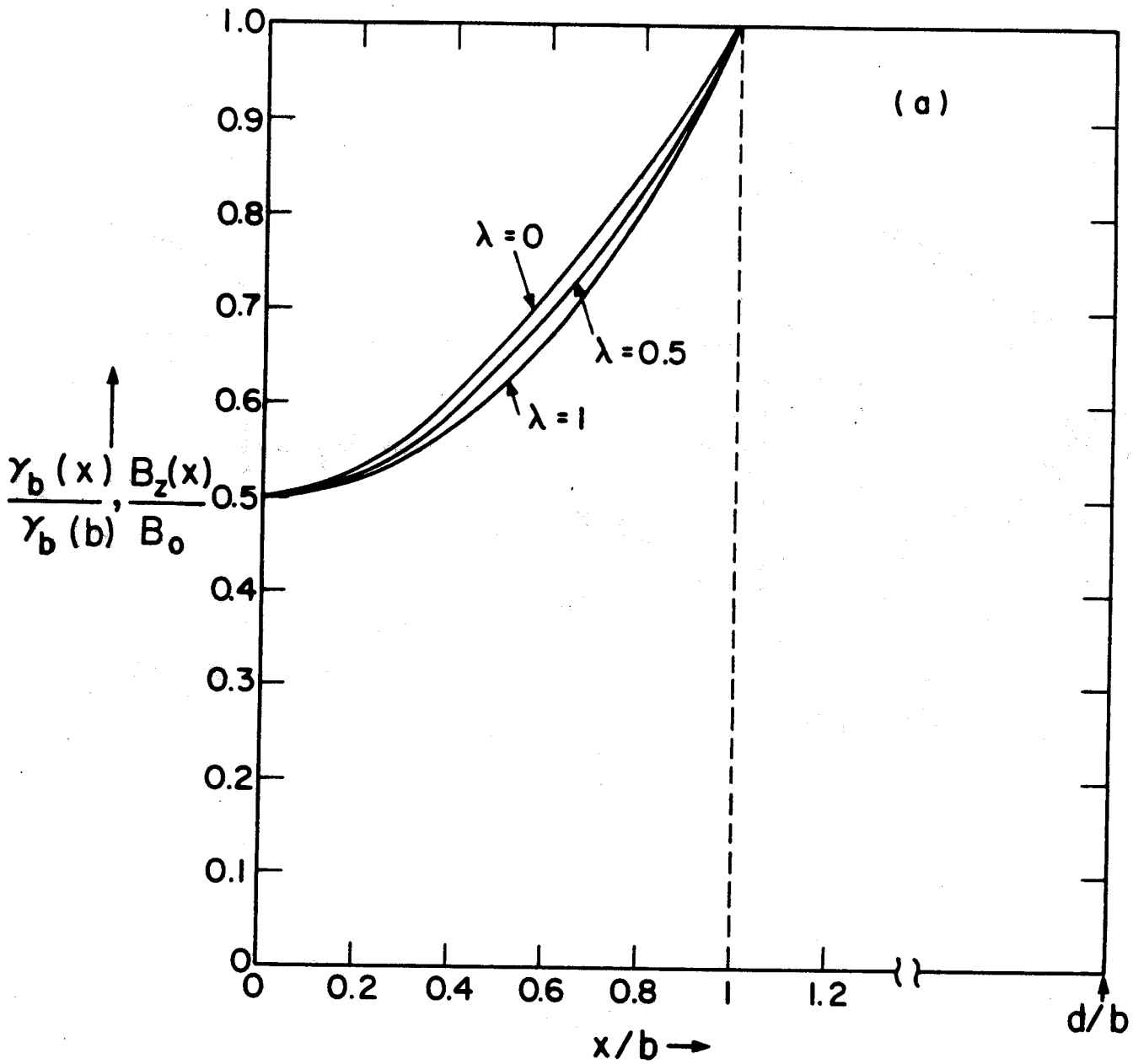
1.0
0.9
0.8
0.7
0.6
0.5
0.4
0.3
0.2
0.1
0
(a)
λ = 0
λ = 0.5
λ = 1
γb (x)/γb (b), Bz(x)/Bo
0
0.2
0.4
0.6
0.8
1
1.2
d/b
x/b

Fig. 2(a)

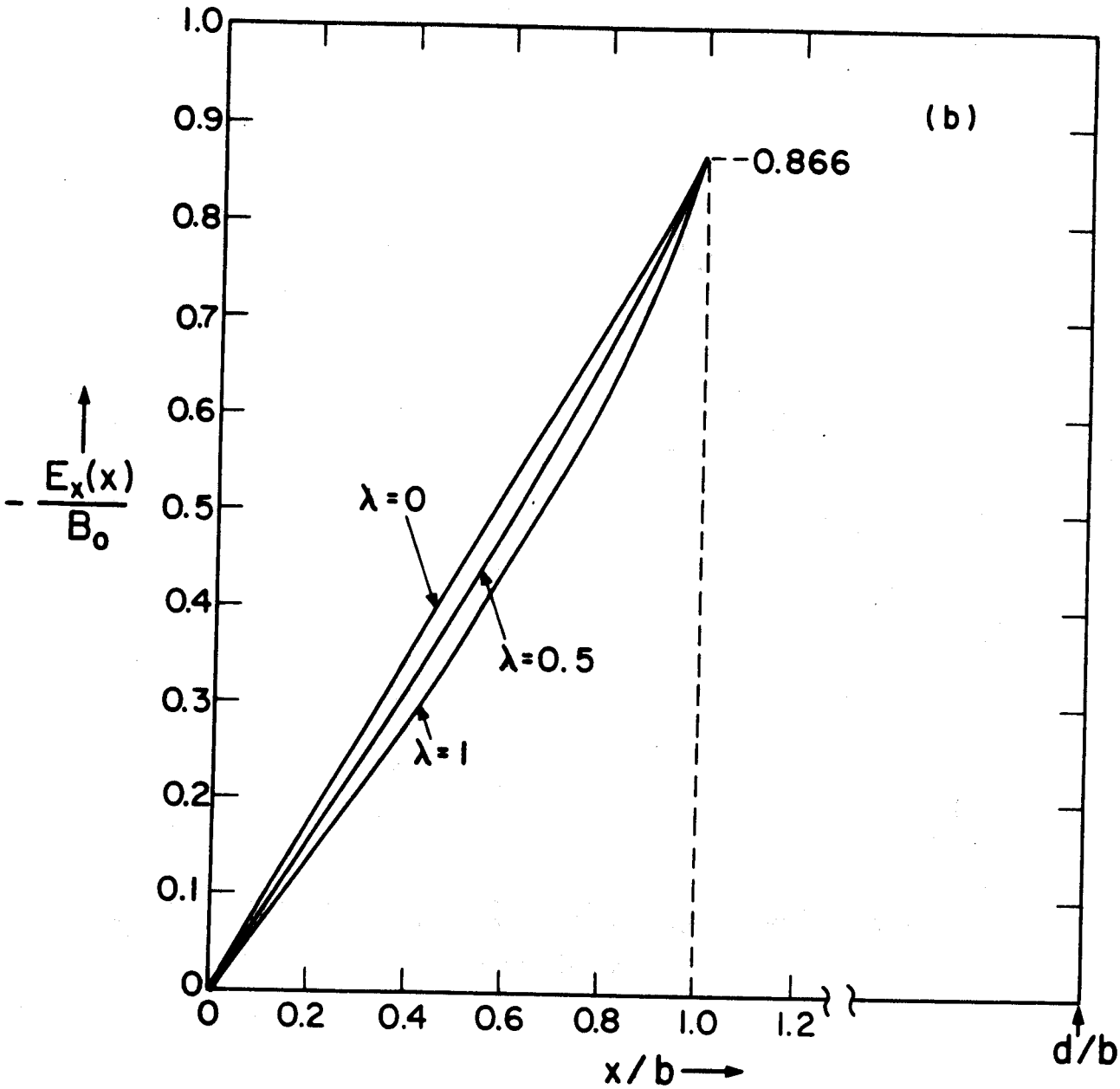
1.0
0.9
0.8
0.7
0.6
0.5
0.4
0.3
0.2
0.1
0
(b)
0.866
$-\frac{E_x(x)}{B_0}$
λ=0
λ=0.5
λ=1
0
0.2
0.4
0.6
0.8
1.0
1.2
x/b
d/b

Fig. 2(b)

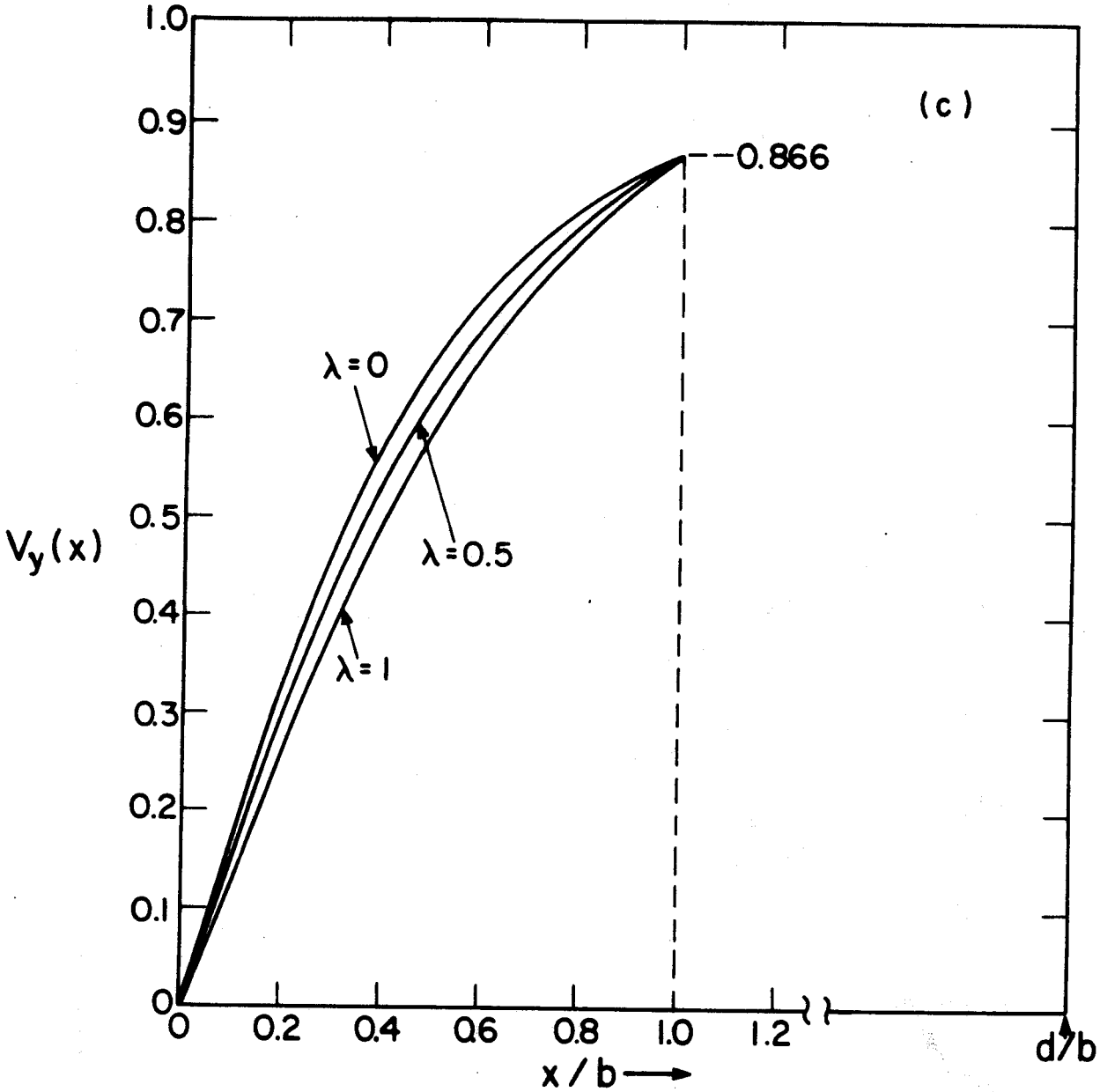
(c)
0.866
λ=0
λ=0.5
λ=1
$V_y(x)$
x / b
d/b
1.0
0.9
0.8
0.7
0.6
0.5
0.4
0.3
0.2
0.1
0
0.2
0.4
0.6
0.8
1.0
1.2

Fig. 2(c)

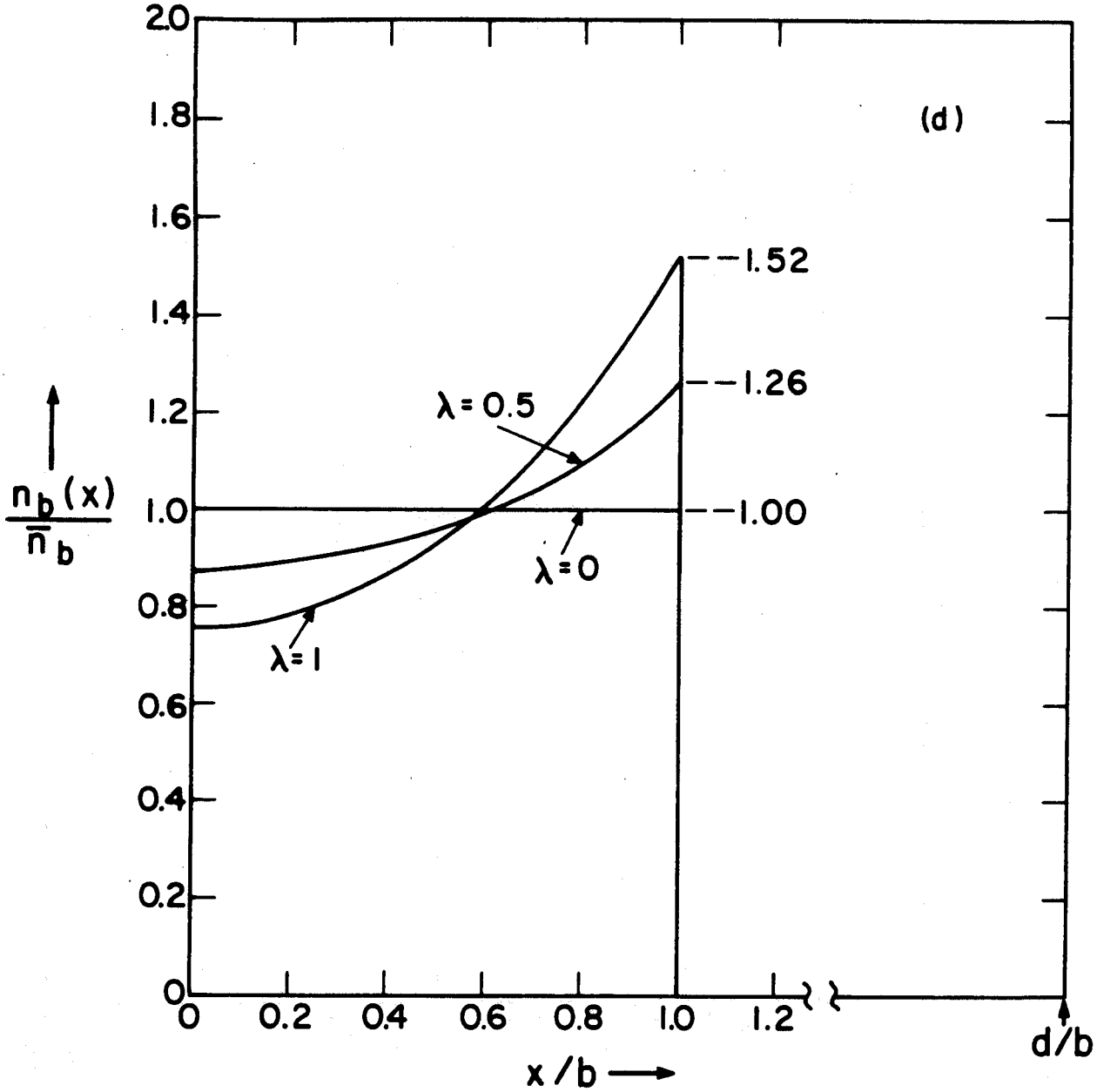
(d)
2.0
1.8
1.6
1.4
1.2
1.0
0.8
0.6
0.4
0.2
0
1.52
1.26
1.00
λ = 0.5
λ = 0
λ = 1
$\frac{n_b(x)}{\bar{n}_b}$
0
0.2
0.4
0.6
0.8
1.0
1.2
d/b
x/b

Fig. 2(d)

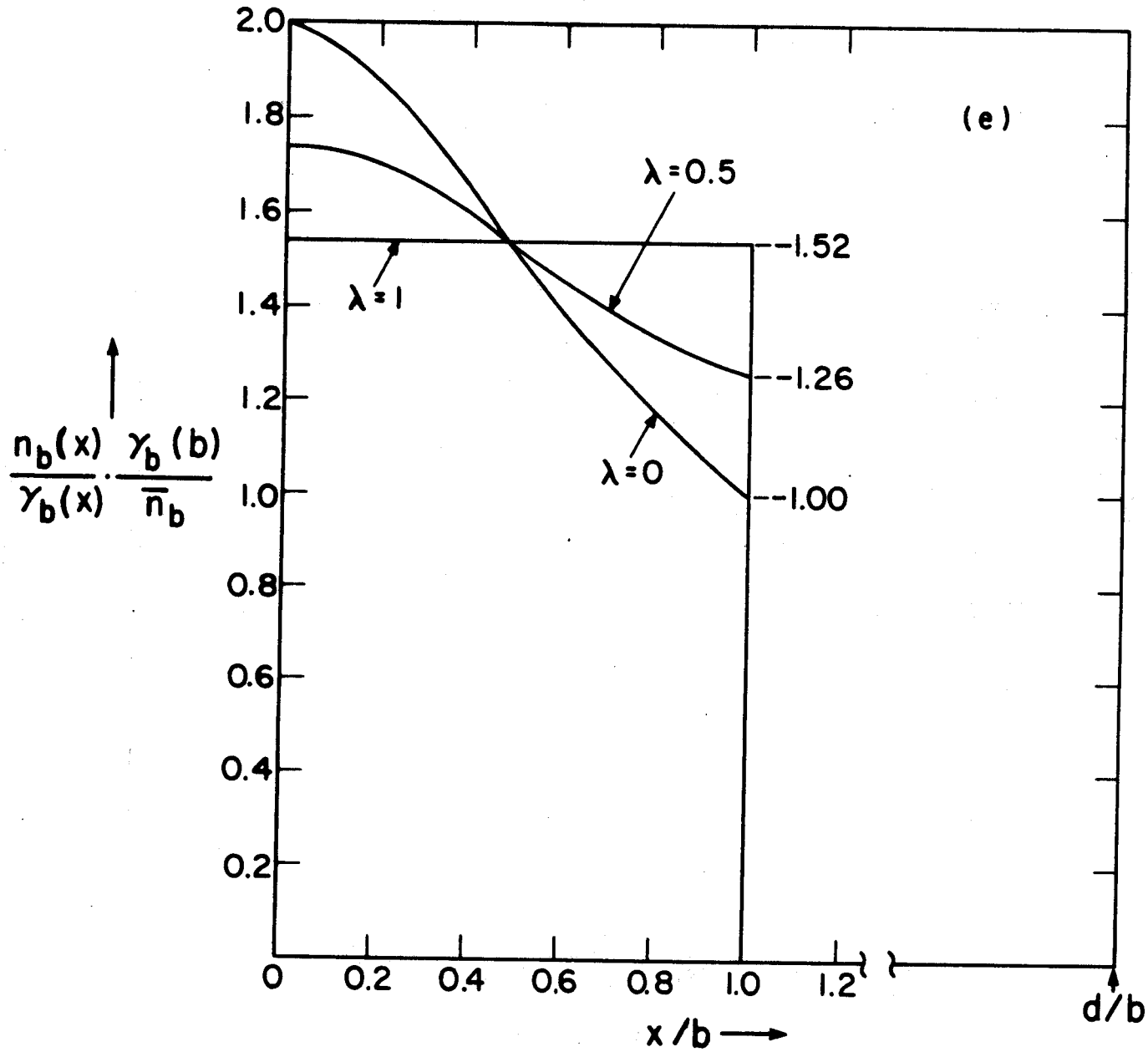
2.0
1.8
1.6
1.4
1.2
1.0
0.8
0.6
0.4
0.2
0
0.2
0.4
0.6
0.8
1.0
1.2
(e)
λ=0.5
λ=1
λ=0
1.52
1.26
1.00
$\frac{n_b(x)}{\gamma_b(x)} \cdot \frac{\gamma_b(b)}{\bar{n}_b}$
x/b
d/b

Fig. 2(e)

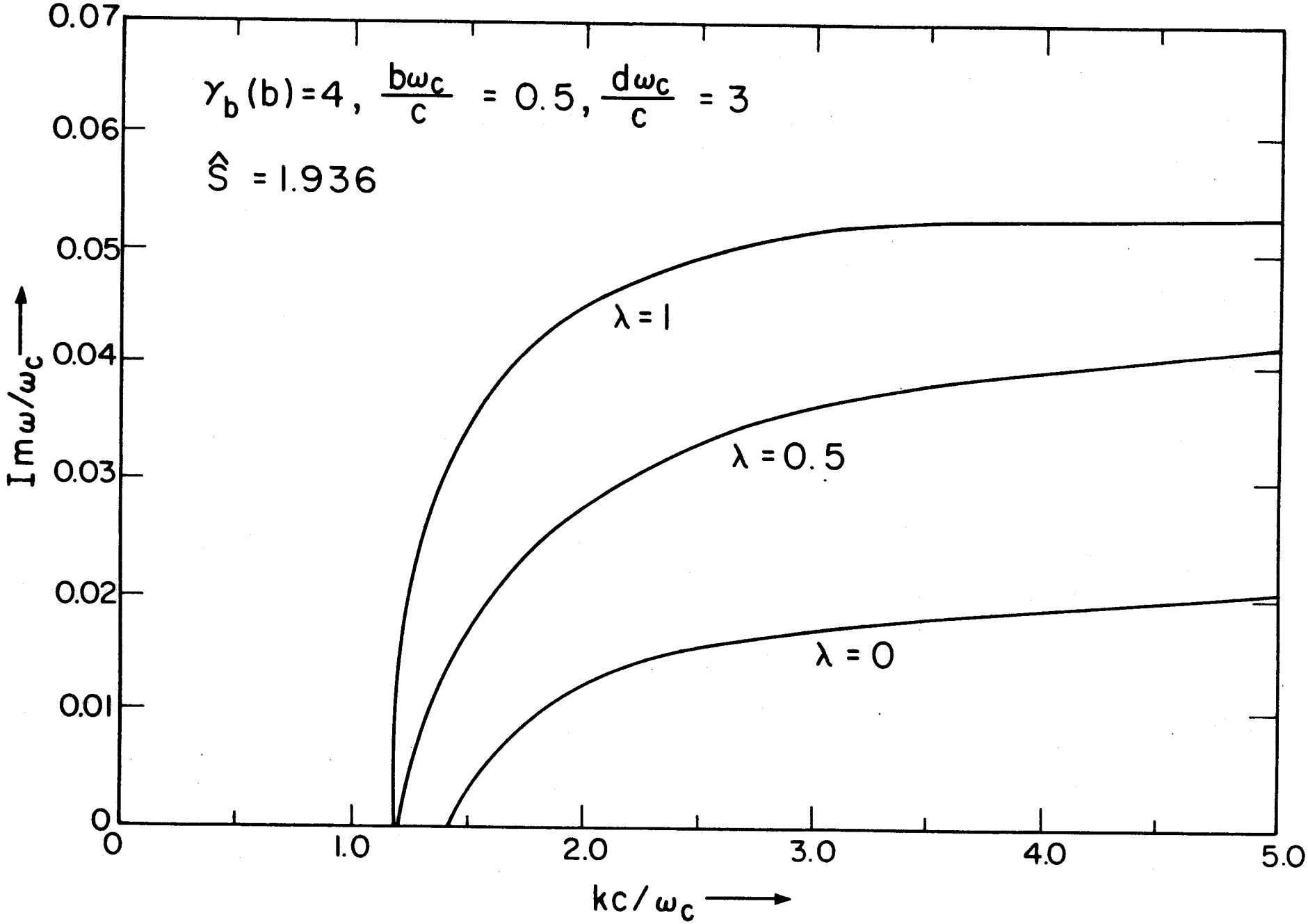
$\gamma_b(b) = 4, \frac{b\omega_c}{c} = 0.5, \frac{d\omega_c}{c} = 3$
$\hat{S} = 1.936$
$\lambda = 1$
$\lambda = 0.5$
$\lambda = 0$
$Im\,\omega/\omega_c$
kc/ω_c
0.07
0.06
0.05
0.04
0.03
0.02
0.01
0
1.0
2.0
3.0
4.0
5.0

Fig. 3

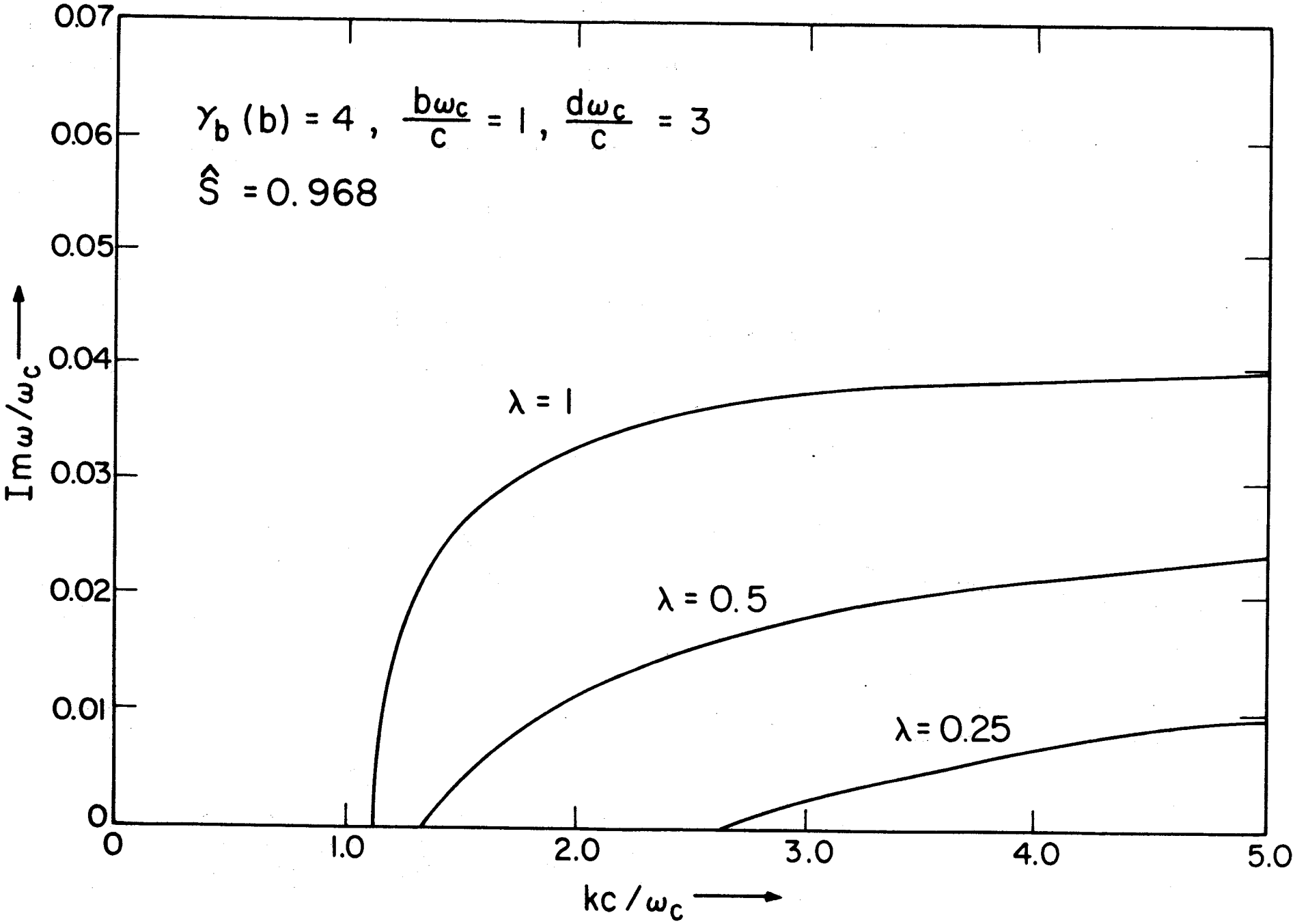
$\gamma_b(b) = 4$, $\frac{b\omega_c}{c} = 1$, $\frac{d\omega_c}{c} = 3$
$\hat{S} = 0.968$
$\lambda = 1$
$\lambda = 0.5$
$\lambda = 0.25$
$Im\,\omega/\omega_c$
kc/ω_c
0.07
0.06
0.05
0.04
0.03
0.02
0.01
0
0
1.0
2.0
3.0
4.0
5.0

Fig. 4

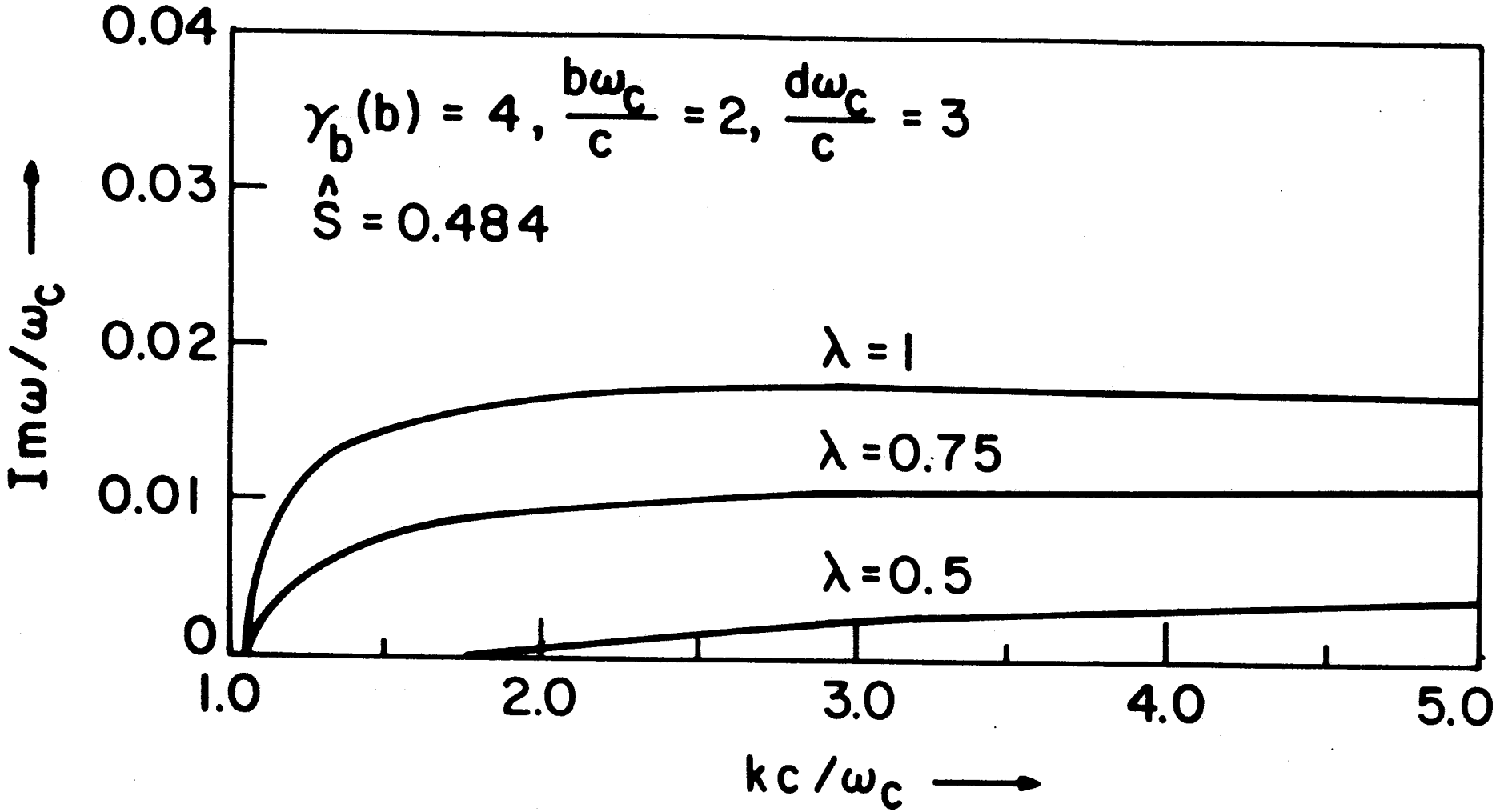
$\gamma_b(b) = 4, \frac{b\omega_c}{c} = 2, \frac{d\omega_c}{c} = 3$
$\hat{S} = 0.484$
$\lambda = 1$
$\lambda = 0.75$
$\lambda = 0.5$
0.04
0.03
0.02
0.01
0
1.0
2.0
3.0
4.0
5.0
$\mathrm{Im}\,\omega/\omega_c$
kc/ω_c

Fig. 5

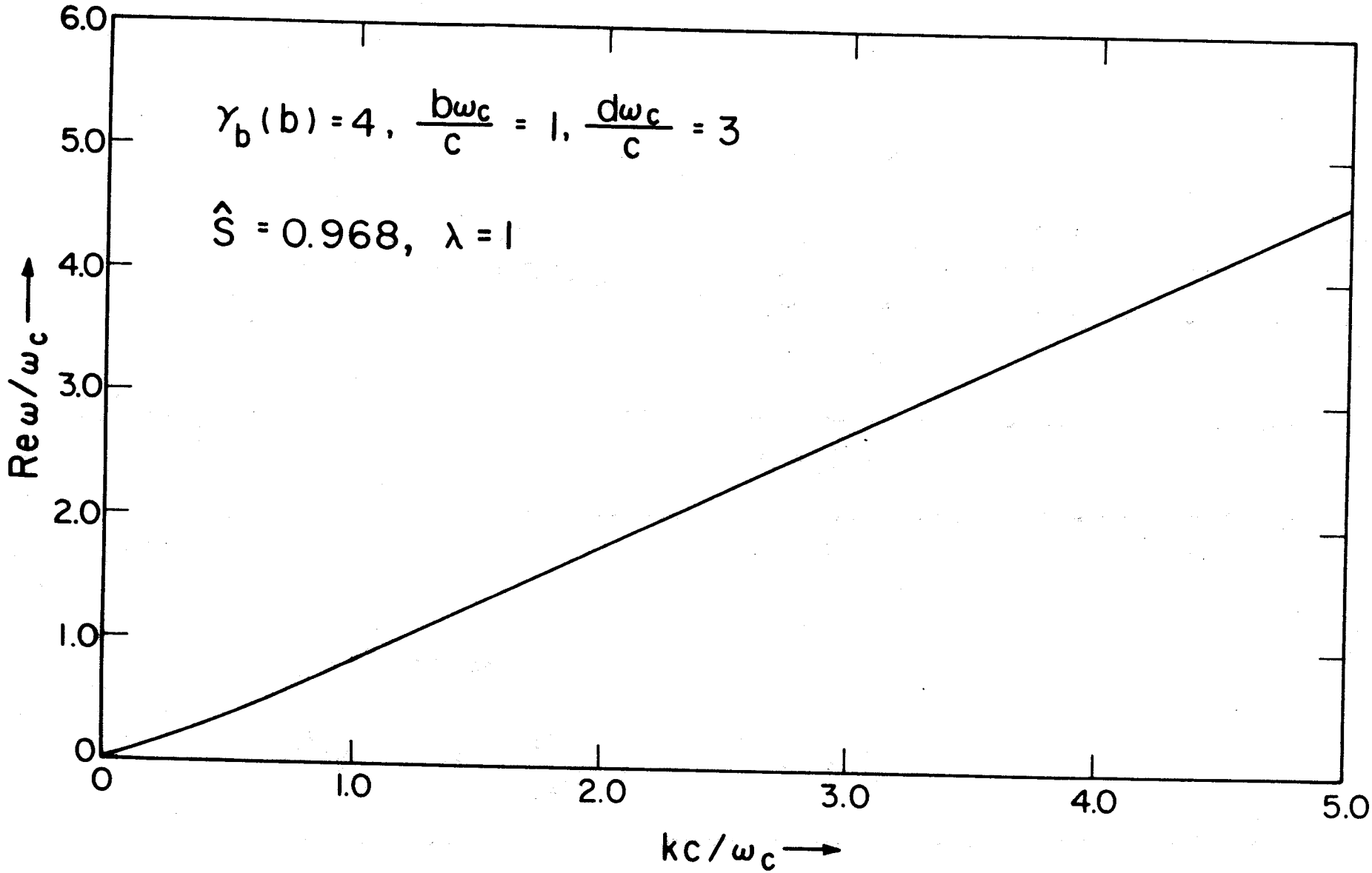
$\gamma_b(b) = 4, \ \frac{b\omega_c}{c} = 1, \ \frac{d\omega_c}{c} = 3$
$\hat{S} = 0.968, \ \lambda = 1$
6.0
5.0
4.0
3.0
2.0
1.0
0
$\mathrm{Re}\,\omega/\omega_c$
0
1.0
2.0
3.0
4.0
5.0
kc/ω_c

Fig. 6

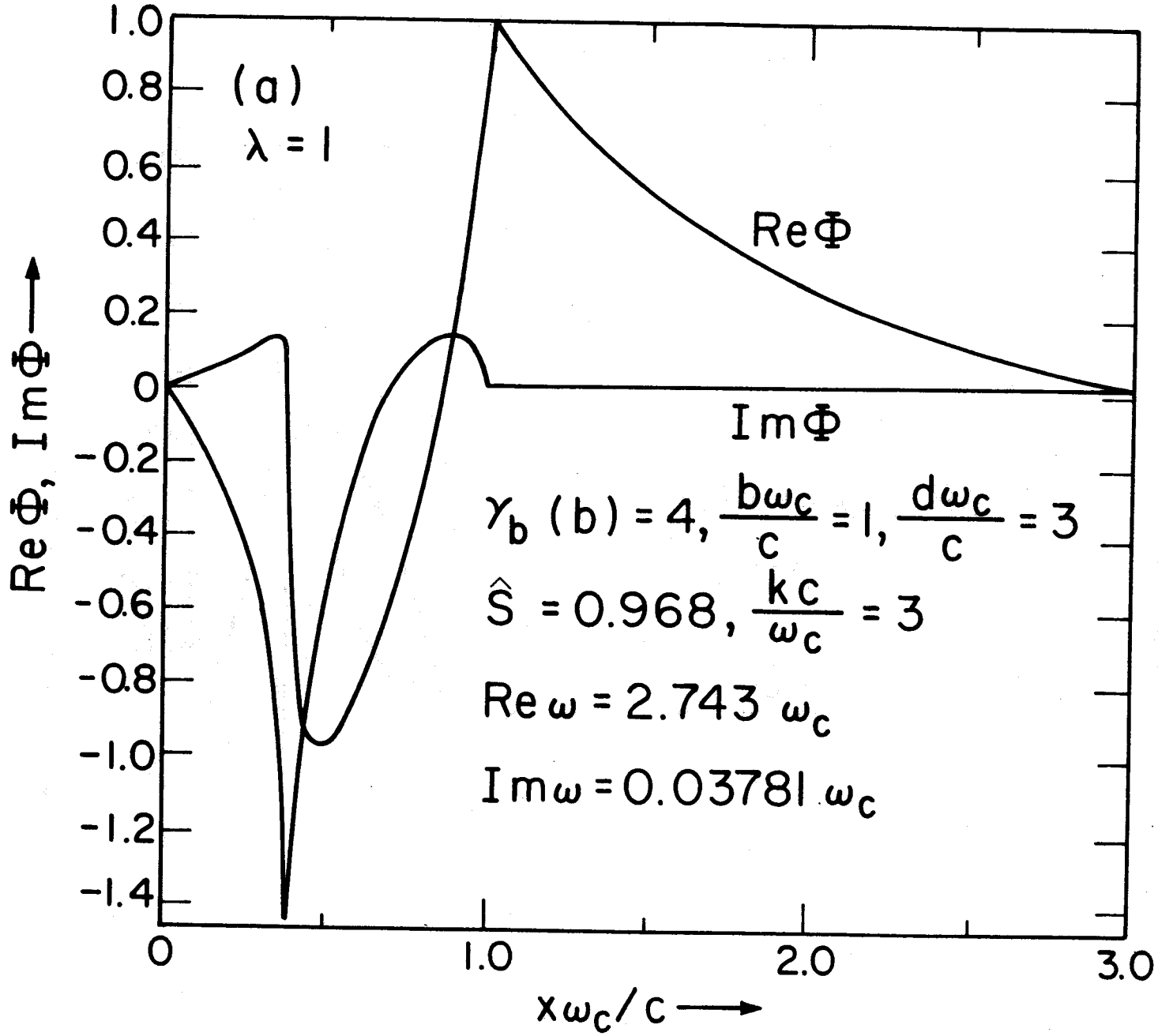
(a)
λ = 1
Re Φ
Im Φ
$\gamma_b(b) = 4, \frac{b\omega_c}{c} = 1, \frac{d\omega_c}{c} = 3$
$\hat{S} = 0.968, \frac{kc}{\omega_c} = 3$
$\mathrm{Re}\,\omega = 2.743\ \omega_c$
$\mathrm{Im}\,\omega = 0.03781\ \omega_c$
Re Φ, Im Φ
$x\omega_c/c$
1.0
0.8
0.6
0.4
0.2
0
-0.2
-0.4
-0.6
-0.8
-1.0
-1.2
-1.4
0
1.0
2.0
3.0

Fig. 7(a)

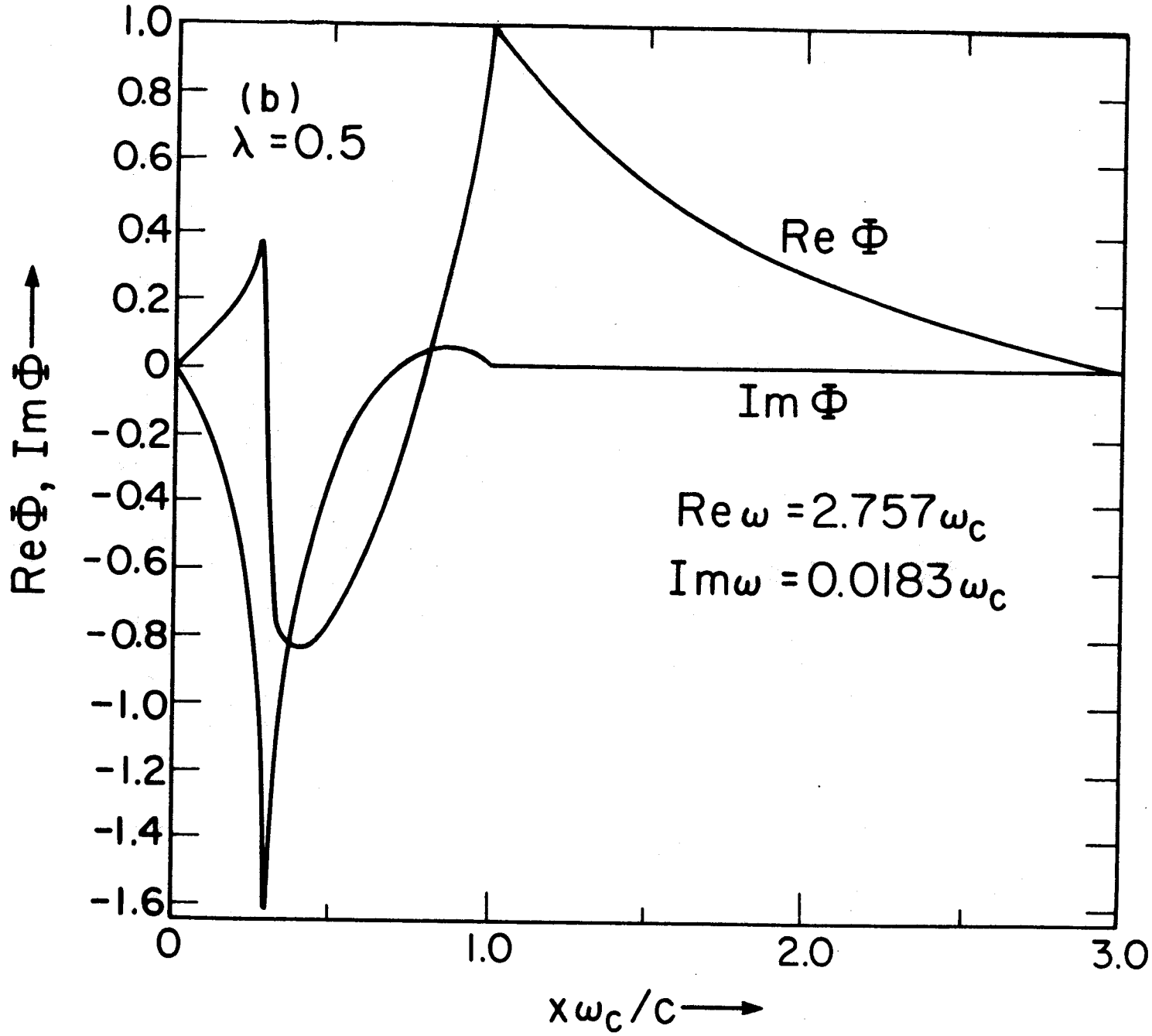
(b)
λ =0.5
Re Φ
Im Φ
Re ω =2.757 ω_c
Im ω =0.0183 ω_c
Re Φ, Im Φ
x ω_c / c
1.0
0.8
0.6
0.4
0.2
0
-0.2
-0.4
-0.6
-0.8
-1.0
-1.2
-1.4
-1.6
0
1.0
2.0
3.0

Fig. 7(b)

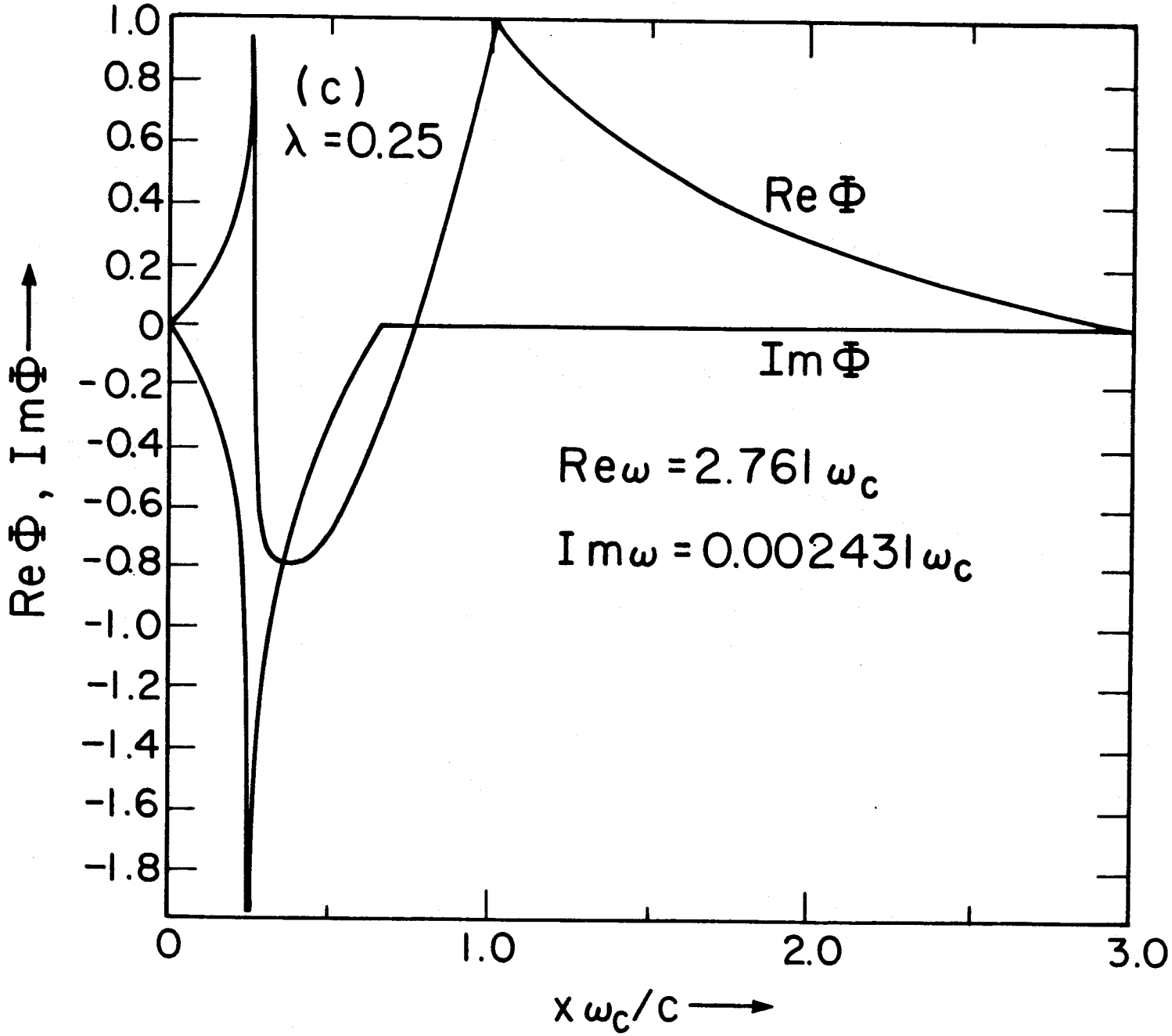
(c)
λ =0.25
Re Φ
Im Φ
Re ω = 2.761 ω_c
Im ω = 0.002431 ω_c
Re Φ , Im Φ
x ω_c / c
1.0
0.8
0.6
0.4
0.2
0
-0.2
-0.4
-0.6
-0.8
-1.0
-1.2
-1.4
-1.6
-1.8
0
1.0
2.0
3.0

Fig. 7(c)

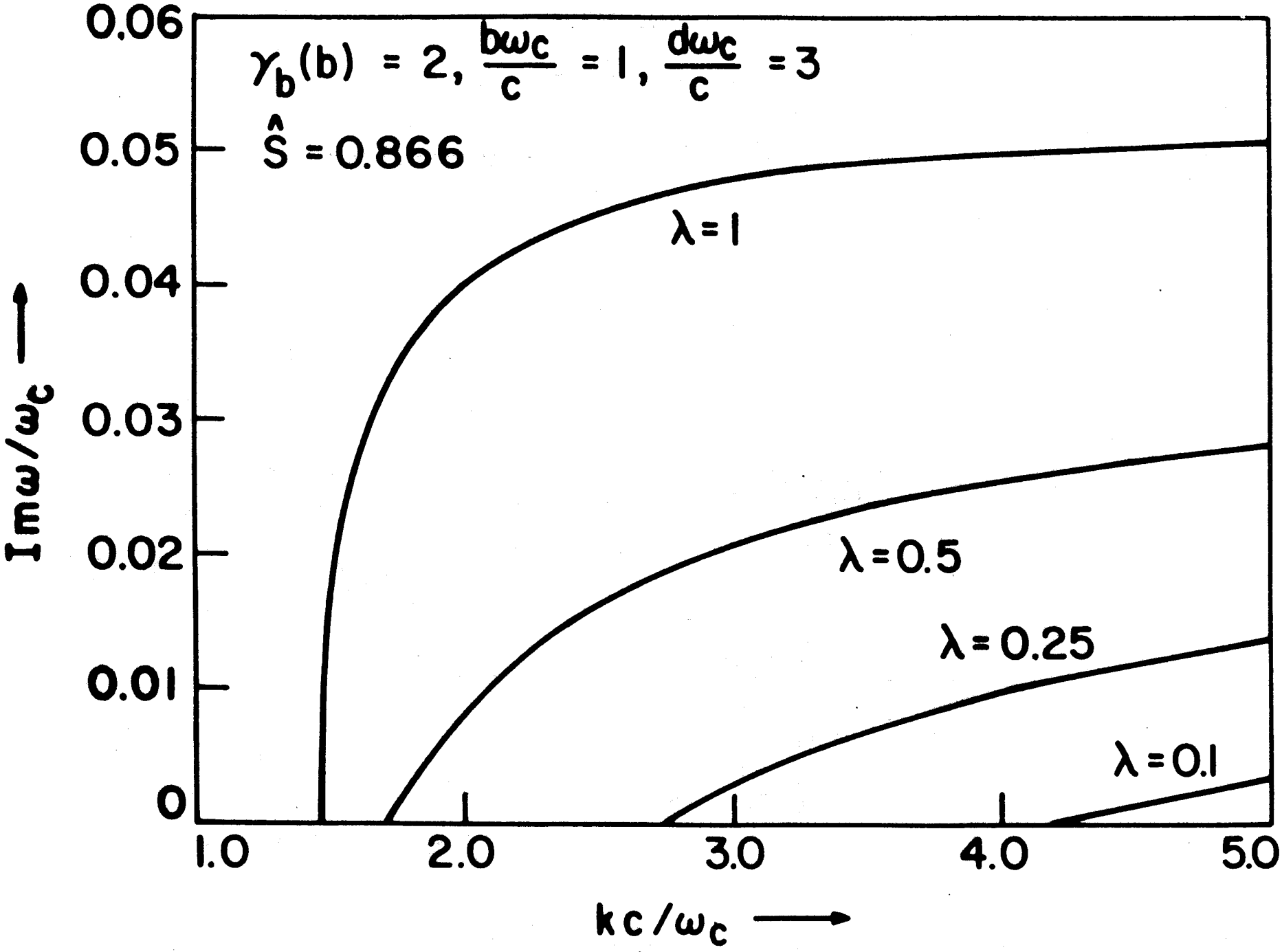
$\gamma_b(b) = 2, \frac{b\omega_c}{c} = 1, \frac{d\omega_c}{c} = 3$
$\hat{S} = 0.866$
$\lambda = 1$
$\lambda = 0.5$
$\lambda = 0.25$
$\lambda = 0.1$
0.06
0.05
0.04
0.03
0.02
0.01
0
$Im\omega/\omega_c$
1.0
2.0
3.0
4.0
5.0
kc/ω_c

Fig. 8

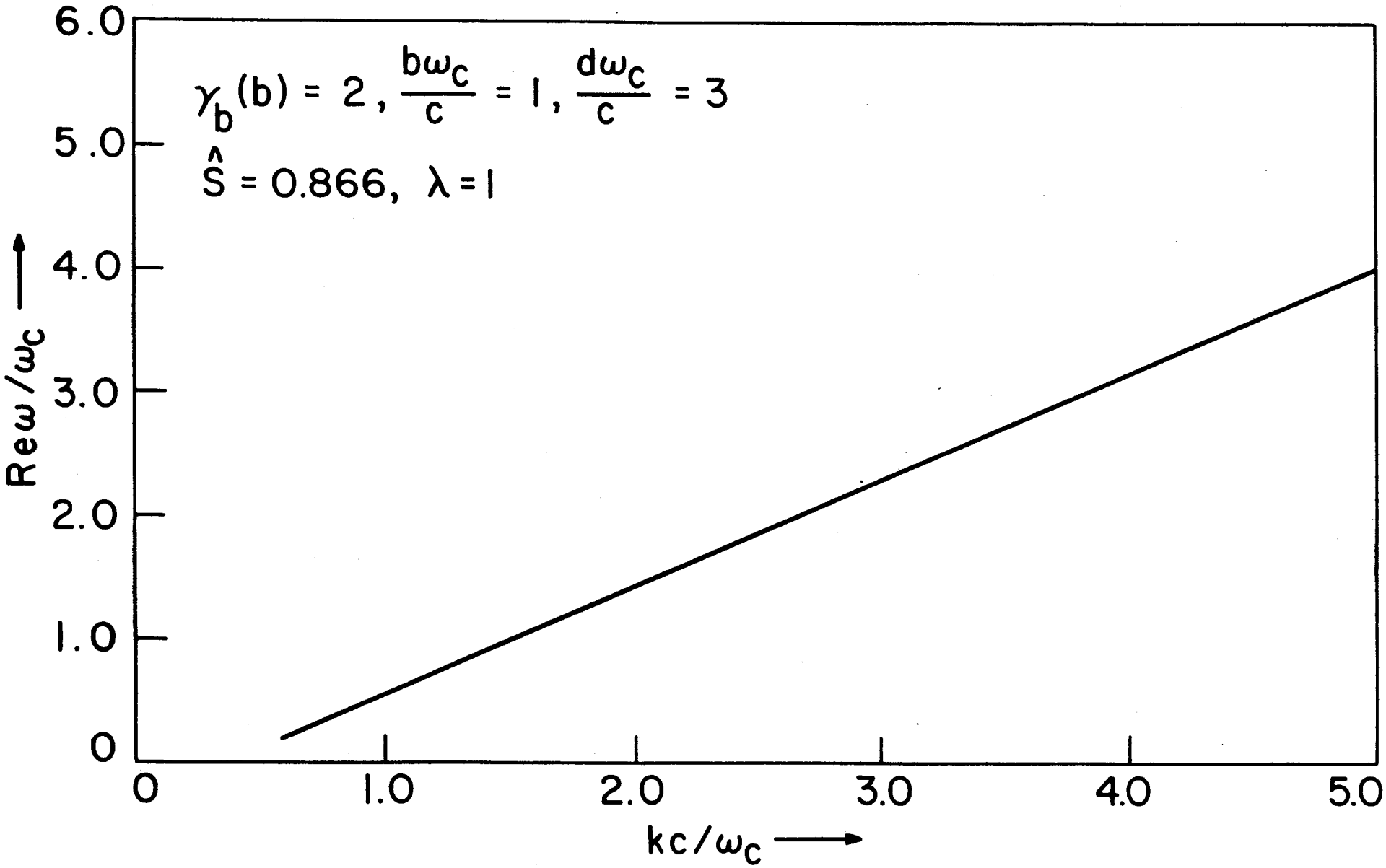
$\gamma_b(b) = 2, \frac{b\omega_c}{c} = 1, \frac{d\omega_c}{c} = 3$
$\hat{S} = 0.866, \lambda = 1$
6.0
5.0
4.0
3.0
2.0
1.0
0
$Re\omega/\omega_c$
0
1.0
2.0
3.0
4.0
5.0
kc/ω_c

Fig. 9